Modelling firebrand transport in wildfires using HIGRAD/FIRETEC

Eunmo Koo[A,D], *Rodman R. Linn*[A], *Patrick J. Pagni*[B] *and Carleton B. Edminster*[C]

[A]Earth and Environmental Sciences Division, Los Alamos National Laboratory,
  Los Alamos, NM 87544, USA.
[B]Mechanical Engineering Department, University of California at Berkeley,
  Berkeley, CA 94720, USA.
[C]Rocky Mountain Research Station, USDA Forest Service, Flagstaff,
  AZ 86001, USA.
[D]Corresponding author. Email: koo_e@lanl.gov

Abstract. Firebrand transport is studied for disc and cylindrical firebrands by modelling their trajectories with a coupled-physics fire model, HIGRAD/FIRETEC. Through HIGRAD/FIRETEC simulations, the size of possible firebrands and travelled distances are analysed to assess spot ignition hazard. Trajectories modelled with and without the assumption that the firebrands' relative velocities always equal their terminal velocities are. Various models for the flight and combustion of disc- and cylindrical-shaped firebrands are evaluated. Eight simulations are performed with surface fuel fires and four simulations are performed with combined surface and canopy fuels. Firebrand trajectories without terminal velocity are larger than those from models with terminal velocity. Discs travel further than cylinders, as discs are aerodynamically more favourable. Thin discs burning on their faces and tall cylinders burning around their circumference have shorter lifetimes than thin discs burning from their circumference or longer cylinders burning from their ends. Firebrands from canopy fires, with larger size and potential to ignite recipient fuel, travel further than firebrands from surface fires. In the simulations, which included a line fire ignition in homogeneous fuels on flat terrain, the firebrand launching patterns are very heterogeneous, and the trajectories and landing patterns are dominated by the coupled fire–atmosphere behaviour.

Additional keywords: coupled-physics fire model, spotting, WUI fires.

Received 25 December 2009, accepted 23 August 2011, published online 9 March 2012

Introduction

Firebrands are burning objects generated by fires, lofted by updrafts caused by fire-induced buoyancy, and transported downwind with the potential to ignite new fires. This discontinuous method of fire spread, referred to as spotting, is difficult to predict and becomes more significant as the intensity and size of a fire increases. This is largely due to the fact that greater intensity translates to stronger local vertical velocities that can loft larger firebrands, and larger fires have larger plumes, so it takes firebrands longer to escape the rising column of air because firebrands tend to be retained within the plume for a longer time (Albini 1979). Thus, firebrand and spotting behaviour can be critical elements of large-scale wildfires, conflagrations and wildland–urban intermix (WUI) area fires such as the 1991 Oakland Hills Conflagration (Pagni 1993). In this catastrophic fire, spotting was the dominant spread mechanism (Woycheese 2000). Fig. 1 shows a firebrand from this fire on 20 October 1991 that is presumed to have been produced from a cedar shingle. When this firebrand was discovered

~1 km west of the perimeter of the Oakland Hills Conflagration, it still displayed glowing combustion.

The behaviour of firebrands can be thought of as a series of three stages: (1) generation or release; (2) lofting and transport; and (3) deposition and subsequent ignition of recipient fuels. The generation of firebrands often involves degradation and physical breakdown of solid material through combustion and ignition of the material. The uncertainty in the processes of dislodging a fragment of combustible material, igniting the particular fragment and then having the specific location and arrangement of the fragment correlate with the timing and location of a gust of wind suggests that a probabilistic approach to firebrand generation would be more feasible than other approaches. Similarly, the processes through which recipient materials are ignited by landing firebrands depends on recipient material type, geometry, condition, etc. As no current model or dataset includes spatially explicit data at the length scales of firebrands (millimetre to metre scales), it would be difficult to handle this process deterministically even if we could model the

exact trajectory and landing location of a firebrand (which is impossible owing to the flight paths' dependence on unknown details of the turbulent wind field and the generation process). Thus, a probabilistic approach seems appropriate for capturing the effect of spotting on the ignition of new fires. Because the details of the generation and subsequent ignition processes are beyond the scope of this paper, firebrands are initiated from any location with sufficient vertical velocity to lift them, and the patterns of landing firebrands are studied. A worst-case scenario would be if all of the burning firebrands that land started spot fires.

Firebrand transport has a significant role in the determination of spot fire hazard because the interaction between the firebrand and the surrounding winds controls the distance and direction of the firebrand's net travel. This interaction determines whether the firebrand will be entrained as well as its flight trajectory, but

Fig. 1. A firebrand from the Oakland Hills Conflagration: $\sim$50-mm diameter, $\sim$5-mm thickness and 2.3 g (density of $\sim$250 kg m^{-3}). The firebrand is presumed to have been produced from a cedar shingle (Koo *et al.* 2010).

it is dependent on the size and shape of the firebrand as well as the nature of the surrounding winds. The lifetime of the firebrand before burning out limits the maximum distance that a particular firebrand can cause spotting. In order to characterise the average properties of firebrand transport (given the enormous number of firebrands that are launched from many fires), some researchers have used quantities like the maximum distance of firebrand travel. The effective spotting distance could also be a measure of the distance that firebrands are carried and deposited with sufficient heat to ignite new fires (requiring information about recipient material conditions).

A significant proportion of the research on spotting hazard over the past five decades has focussed on firebrand transport, as shown in Table 1. A detailed review of the previous firebrand research is available in Koo *et al.* (2010) However, that paper reviewed literature that was published by 2007, and there are recent studies that should be mentioned. Sardoy *et al.* (2008) simulated disc firebrands with different aspect ratios in a boundary-layer wind field using a one-seventh-law wind profile and an integral plume model to find the bimodal ground-level distribution of landed firebrands. Kortas *et al.* (2009) modelled cylindrical and disc-shaped firebrands produced from the firebrand generator, an experimental apparatus designed by Manzello *et al.* (2008*b*), for validation of their model. Though their study did not simulate the fire scenarios, it is a valuable investigation because it deals with model validation, which is extremely difficult for firebrand models. Wang (2011) studied generation and transport of firebrands with an analytical approach. The study also used a statistical pattern for downwind distribution of firebrands. This study analysed effect of firebrands on the Canberra bushfire of 2003. Ellis (2010) performed an experimental study of the aerodynamic behaviour of jarrah flakes and karri bark as potential firebrands. In order to study the nature of the firebrand behaviour, these kinds of statistical approaches and experimental studies are important as well as physical modelling studies.

The firebrand simulation experiments in this work have evolved from several of these firebrand studies. As shown in Table 1, many of the prior studies used simplified plume and

Table 1.   Compendium of selected firebrand models by 2007, excerpt from Koo *et al.* (2010)

Author	Year	Firebrand model	Plume and wind model
Tarifa *et al.*	1965–67	Sphere, cylinder with combustion	Given launching height in constant horizontal wind, inclined convective plume (Nielsen and Tao 1965)
Lee and Hellman	1969–70	Spheres with combustion (1970)	Turbulent swirling natural convective plume (1969)
Muraszew and Fedele	1974–77	Statistical model (1976)	Fire whirl (1977)
Fernandez-Pello and Tse (and Anthenien)	1982, 1998, 2006	Sphere with combustion (Fernandez-Pello 1982). Disc, cylinder and sphere (2006)	Given launching height (1998), McCaffrey plume (2006) in constant boundary layer wind
Albini	1979–83	Cylinder with combustion (Muraszew and Fedele 1976)	Launching height from flame structure analysis in constant horizontal wind
Woycheese and Pagni	1996–2000	Non-dimensional model with combustion (Kinoshita *et al.* 1981)	Baum and McCaffrey plume model (Baum and McCaffrey 1989)
Himoto and Tanaka	2005	Disc without combustion	Given launching height in turbulent boundary layer
Porterie *et al.*	2007	Small world network model (Porterie *et al.* 2007), Disc with combustion (Sardoy *et al.* 2007)	Steady-state crown fire (Porterie *et al.* 2005)
Koo, Pagni and Linn	2007	Disc and cylinder with combustion	HIGRAD/FIRETEC wildfire model (Linn and Cunningham 2005; Linn *et al.* 2005)

wind-field models (Tarifa *et al.* 1965*a*; Muraszew and Fedele 1976; Albini 1979; Woycheese *et al.* 1999) and divided the transport process into a lofting and a propagation stage. Other spotting models used previously have only a lofting stage (Lee and Hellman 1969) or a propagation stage (Tse and Fernandez-Pello 1998; Himoto and Tanaka 2005). It is important to examine the ramifications of making such distinctions between the lofting and propagation stages. Past research has found that the maximum spot fire distances are obtained from firebrands whose flight time is equal to their lifetime, i.e. firebrands that land at burnout (Tarifa *et al.* 1965*a*; Muraszew and Fedele 1976; Albini 1979; Woycheese *et al.* 1999). By integrating a spotting model, an atmospheric dynamics model and firebrand combustion, it is possible to further investigate this finding.

Previous firebrand models that used simplified wind fields for firebrand transport have assumed that the relative velocity of firebrands with respect to local winds is always equal to their terminal velocity (Tarifa *et al.* 1965*a*). This assumption implies that the drag forces and body forces (gravity) are perfectly balanced at all times and the relative velocity can therefore be calculated based on the geometry of the firebrand. This is reasonable in the context of simplified wind fields, and is supported by wind-tunnel tests where strong transients or spatial heterogeneities do not exist in the wind fields (Tarifa *et al.* 1965*a*). However, if the time scale of changes in the winds surrounding the firebrands is shorter than the response time of the firebrand to adjust its velocity to the terminal velocity, which was observed as 2 to 3 s in Tarifa's wind-tunnel experiments (Tarifa *et al.* 1965*a*), this assumption may induce errors. In general, as area per weight and therefore drag per weight increases as firebrand size gets smaller, the terminal velocity approximation is likely to be more appropriate for smaller firebrands and less appropriate for larger ones because the ratio of surface area to mass increases as firebrand size diminishes, which leads to a shorter response time for firebrand velocity. It is important to examine the implications of using this terminal velocity approximation for firebrand transport, especially in the vicinity of highly turbulent fire-influenced plumes.

It was determined that for spherical firebrands capable of carrying enough heat to be effective firebrands, the surface area per unit weight or drag per unit weight was too small (Woycheese 2000). The spherical model of firebrands has the highest volume/surface ratio, so it is actually the most difficult shape of a given mass to loft. Thus, discussions of spherical firebrand models are not included in this paper. Thin discs and long cylinders both have larger drag per weight ratios. In addition, thin discs and long slender cylinders are fairly representative of natural firebrands larger than a millimetre. Discs can represent firebrands generated from wooden materials in structures, such as wood shingles, as shown in Fig. 1. Firebrands generated from trees (Manzello *et al.* 2008*a*) and vegetation can be modelled as cylinders.

Burning firebrands lose mass owing to combustion during their flight. The resulting changes in the geometry alter their aerodynamic characteristics, which then affects their trajectories and travel distance. In addition, many of the firebrands that are launched burn out during the flight. Therefore, the evolution in shape and combustion of firebrands plays an important role in determining the spotting distance. Theoretically, the maximum loftable initial size of a firebrand is limited by the strength of the updrafts in the original fire. Thus, fuel conditions at the location of firebrand generation affect firebrand transport by limiting the size of firebrands to be launched.

Though many previous studies have separated lofting by buoyant plume and propagating with prevailing winds or used buoyant plume models superimposed on simplified ambient wind fields, the interaction of the prevailing wind and the fire-induced buoyant plume is in fact a complex phenomenon. For this study, wind fields generated by HIGRAD/FIRETEC, a coupled-physics wildfire model developed at Los Alamos National Laboratory (LANL), provide detailed wind-field data including turbulence (Linn 1997). In the present paper, several firebrand models (thin discs and long cylinders) are developed and their transport trajectories are studied in the context of these coupled fire–atmosphere wind fields. These firebrand models consist of formulations for drag and lift forces on the firebrands as a function of geometry, relative wind velocity and combustion. Firebrand transport is studied with and without terminal velocity assumptions, in the context of fires in surface fuel beds and in surface and canopy fuel complexes.

Model description

Though firebrands can have a wide variety of complex shapes in reality, the current modelling approach focusses on firebrands that can be loosely represented by two simple firebrand shapes with defined orientations, a disc and a cylinder. This subset of possible shapes is used for model and computational tractability, with the assumption that these shapes are fairly representative of a large fraction of firebrands from vegetation and firebrands originating from structures. In this section, models are developed for the evolution and flight characteristics of thin disc and long cylindrical firebrands. These models include elements describing the combustion and resulting evolution of firebrand shape as well as elements modelling the balance between gravity, lift and drag forces on a firebrand. In order to assess the effect of the terminal velocity assumption, dynamics models based on force balance with and without this assumption are developed and tested. The formulations and their implications are described in this section.

Force balance with terminal velocity assumption

Discs and cylinders have the same basic geometry with different height-to-radius ratios. Thus, their volume can be expressed in the same way, $V = \pi r^2 h$ where h is the thickness or length and r is the radius. Their cross-section area, which is related to their primary orientation to the wind, could be either πr^2 or $2rh$. Their orientation with respect to the relative wind must be considered differently based on the difference in their free-falling stability. Tarifa *et al.* (1965*a*) found in free-falling tests that disc and cylindrical firebrands' velocities remain reasonably stable at specific orientations during flight. When the height-to-radius ratio is less than ~0.5 (disc), then the cross-section area should be πr^2 and when the height-to-radius ratio is greater than ~5 (cylinder), then the cross-section area should be $2rh$, as shown in Fig. 2. The firebrands are assumed to be always stable in the
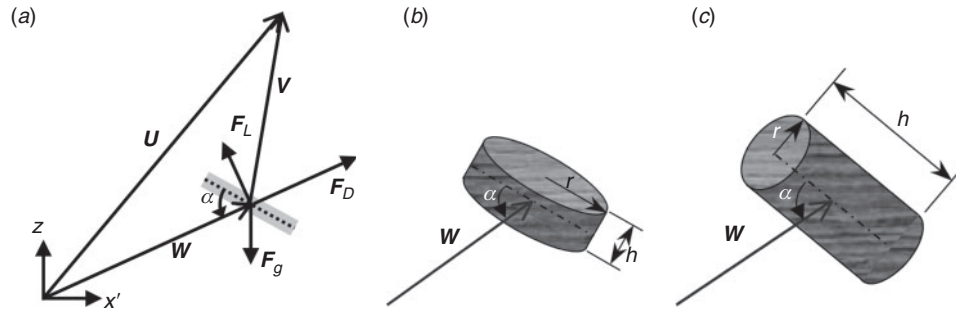
Fig. 2. (*a*) A schematic of forces on a firebrand moving at terminal velocity with respect to the wind: a firebrand model with orientation, e.g. (*b*) a disc or (*c*) a cylinder. The angle of attack is defined from different reference lines as shown.

position of maximum drag. This is done in order to determine maximum spot fire distance.

Fig. 2*a* shows a schematic of forces on a disc or cylindrical firebrand in a wind reference frame. *z* is the vertical direction and x' is the horizontal direction aligned with the local wind velocities. In other words, the firebrand is at an instant where it is immersed in a flow that can locally be described in an x'–z plane, but the x' direction is specific to that point in time and space. In this context, the three-dimensional forces acting on the firebrand also lie within the two-dimensional x'–z plane.

This two-dimensional representation assumes that the longer axis of the firebrand, which defines the orientation of the firebrand, is always perpendicular to the x'–z plane that contains the instantaneous relative wind velocity vector; thus, it ignores tumbling or wobbling. W is the wind velocity relative to the firebrand, which is generally different from the flow velocity relative to the ground (U) or the firebrand velocity relative to the ground (V). The wind velocity relative to the firebrand, subsequently called relative velocity, is equal to the difference between the local wind velocity and the actual velocity of the firebrand, $W = U - V$. The angle of attack (α) is the angle between W and the firebrand orientation (shown as a dotted line in Fig. 2).

The firebrand is acted on by its own weight, which is the gravity force (F_g) and the pressure force induced by the flow around the firebrand. The pressure force can be decomposed into two component forces: the drag force (F_D) which is aligned with the relative wind and the lift force (F_L) which is normal to the relative wind. Thus, there are three forces acting on a firebrand in flight: gravity force, drag force and lift force. These forces are determined as follows:

Drag force:

$$F_{D,x'} = \frac{1}{2} A_c \rho_a C_D |W| W_{x'} \tag{1a}$$

$$F_{D,z} = \frac{1}{2} A_c \rho_a C_D |W| W_z \tag{1b}$$

Lift force:

$$F_{L,x'} = -\frac{1}{2} A_c \rho_a C_D |W| W_z \tag{2a}$$

$$F_{L,z} = \frac{1}{2} A_c \rho_a C_D |W| W_{x'} \tag{2b}$$

Gravity force:

$$F_{g,x'} = 0 \tag{3a}$$

$$F_{g,z} = -mg = -\rho_s V_s g \tag{3b}$$

where A_c is the cross-section firebrand area (or projected area), ρ is the density, C_D is the drag coefficient, C_L is the lift coefficient, V_s is the volume of the firebrand, m is the mass of the firebrand, g is the acceleration due to gravity and the subscripts *a* and *s* indicate air and solid. Fig. 2*b* and 2*c* shows a disc firebrand and a cylinder firebrand with different definitions of the angle of attack. For the disc, α is the angle between the plane and W and the cross-section area is πr^2. For the cylinder, α is the angle between its axis and W, and the cross-section area is $2rh$. Drag and lift coefficients are assumed to be the two components of the normal pressure coefficient (C_N) (Hoerner 1958):

$$C_D = C_N \sin \alpha \tag{4a}$$

$$C_L = C_N \cos \alpha \tag{4b}$$

These velocity vector and force conventions were first used for firebrand transport research by Tarifa *et al.* (1965*a*, 1965*b*, 1967), and formed the basis of most firebrand research that followed these early works. Tarifa also established the important assumption that firebrands in flight travel at their terminal velocities with respect to the wind. When a free-falling object is at its terminal velocity in a static homogeneous wind field, its acceleration is zero because the sum of the external forces (pressure and body) acting on the object is assumed to be zero, or:

$$\frac{d}{dt}(mV) = \sum_i F_i = 0 \tag{5}$$

For the sum of forces defined by Eqns 1, 2, 3 and 4, the terminal velocity approximation yields:

$$\frac{1}{2} A_c \rho_a |W| C_N (W_{x'} \sin \alpha - W_z \cos \alpha) = 0 \tag{6a}$$

$$\frac{1}{2} A_c \rho_a |W| C_N (W_z \sin \alpha + W_{x'} \cos \alpha) - mg = 0 \tag{6b}$$

Eqn 6 is the governing equation of firebrand dynamics for all shapes under the terminal velocity assumption. For spheres, which have no preferential direction, $\alpha = 90°$.

The relative wind velocity W can be solved from the force balance Eqn 5. For discs, the components of the relative wind velocity, $W_{x'}$ and W_z are:

$$W_{x'} = \cos \alpha \sqrt{2 \frac{\rho_s}{\rho_a} \frac{hg}{C_N}} \tag{7a}$$

$$W_z = \sin \alpha \sqrt{2 \frac{\rho_s}{\rho_a} \frac{hg}{C_N}} \tag{7b}$$

and for cylinders:

$$W_{x'} = \cos \alpha \sqrt{\pi \frac{\rho_s}{\rho_a} \frac{rg}{C_N}} \tag{8a}$$

$$W_z = \sin \alpha \sqrt{\pi \frac{\rho_s}{\rho_a} \frac{rg}{C_N}} \tag{8b}$$

As drag forces depend strongly on shape, C_N is found for each case using pre-existing data. Various researchers have performed experiments for determining C_N for simple body shapes like discs and cylinders, and Fig. 3 shows Hoerner's (1958) work summarising such efforts. Fig. 3*a* shows that for discs, C_N is constant at 1.17 if the angle of attack is between 35 and 90°. In Fig. 3*b*, C_L and C_D for cylinders are shown. Note that C_L and C_D are functions of the angle of attack and C_N in Eqn 4 whereas C_L and C_D in Fig. 3*b* follow the cross-flow principle defined by $C_N = C_{90°} \sin^2 \alpha$, where $C_{90°}$ is the pressure coefficient when $\alpha = 90°$. The friction drag coefficient of the cylinder, 0.02 in Fig. 3*b*, is ignored here. When the height-to-radius ratio is ~ 10, $C_{90°} \approx 0.7$ (White 1999). As the height-to-radius ratio goes to infinity, $C_{90°} \approx 1.1$, as shown in Fig. 3*b* (Hoerner 1958).

With the equations listed above, W can be calculated. For a given local value of U, which is obtained at each position from HIGRAD/FIRETEC, the firebrand velocity (V) can be calculated by subtracting relative wind velocity (W). The position of a firebrand can be traced by obtaining the distance travelled during Δt using the equations:

$$\Delta x' = \int_t^{t+\Delta t} (U_{x'} - W_{x'}) dt \tag{9a}$$

$$\Delta z = \int_t^{t+\Delta t} (U_z - W_z) dt \tag{9b}$$

Again, with the terminal velocity assumption, there is an assumed balance between the instantaneous and local pressure forces and body forces. For numerical implementation purposes, this is expanded to say that this balance remains constant over the duration of a time step Δt. After each time step, a new firebrand position and evolved wind field provide a new U and thus a new W is calculated.
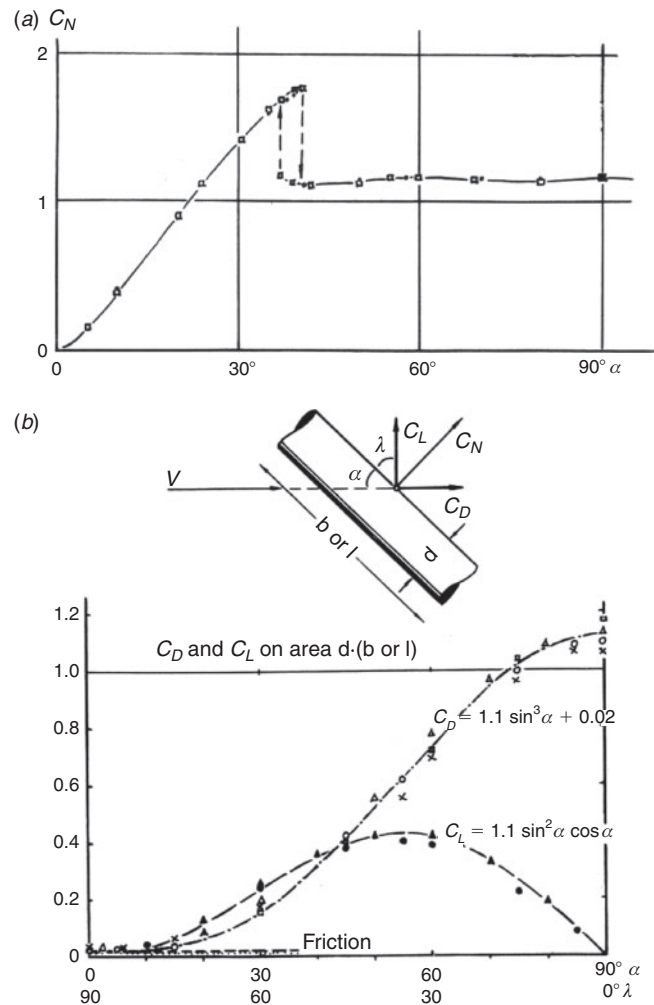

Fig. 3.   (*a*) Normal pressure coefficient (C_N) for discs and (*b*) drag and lift coefficients (C_D and C_L) for infinite cylinders such as wires and cables, shown as functions of the angle of attack (α). From fig. 29*a* (pp. 3–16) and fig. 18 (pp. 3–11) in Hoerner (1958), reproduced with permission.

Forces and acceleration without the terminal velocity assumption

The model described above was based on the terminal velocity assumption established by Tarifa from his observations of firebrand-burning tests in a wind tunnel (Tarifa *et al.* 1965*a*). Tarifa observed that it took only 2 to 3 s for a firebrand to adjust its velocity to its terminal velocity in the wind tunnel. He considered 2–3 s of start-up time as a short enough time to be ignored. This time decreases as the size or density of the firebrand decreases. Thus, Tarifa assumed that a flying firebrand adjusts to its terminal velocity immediately. The terminal velocity postulate has been assumed to be true in many other studies (Lee and Hellman 1969, 1970; Muraszew 1974; Muraszew *et al.* 1975; Muraszew and Fedele 1976, 1977; Albini 1979, 1981, 1982, 1983*a*, 1983*b*; Woycheese 1996, 2000; Woycheese *et al.* 1998, 1999; Himoto and Tanaka 2005). However, this assumption implies that the time scale of the local wind change is larger than the start up time (2 to 3 s for the tested firebrands). There are two basic ways that the local winds change around a firebrand: (1) the
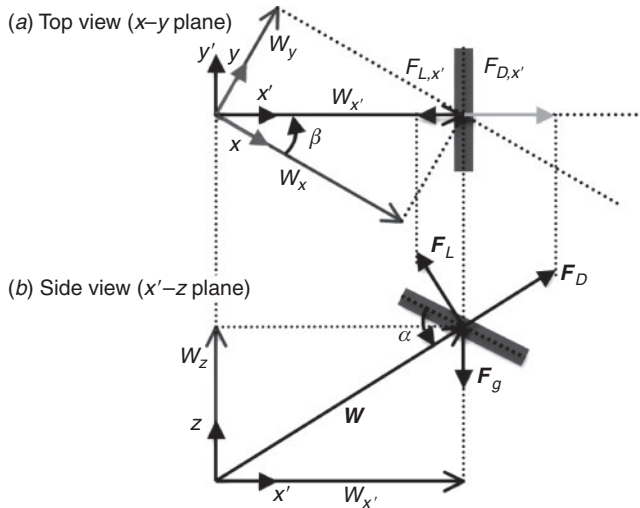
Fig. 4. Firebrand schematic in 3-D. (*a*) Top view on *x*–*y* plane and (*b*) side view on *x*′–*z* plane. *x*′ and *y*′ are the principal directions of relative wind; *x* and *y* are normal static reference coordinate axes on the horizontal plane, which are used in simulations, and *z* is in the vertical direction.

winds evolve in a transient manner; or (2) the firebrand moves from a location with one wind condition to another with a different wind condition. The time scale of the local wind change therefore depends on the spatial heterogeneity of the wind field and the velocity of the firebrand or the rate at which the velocity field evolves. In the presence of a turbulent plume emanating from a fire, the time scales of wind change could be much shorter than 2 s, especially near the edge of the plume. If the wind speed keeps changing, then the relative velocity of the firebrand will be adjusted towards its terminal velocity to reach its equilibrium. However, the wind could change again before the firebrand reaches terminal velocity, so the adjustment process (acceleration or deceleration) would be continuous.

Without the terminal velocity assumption, the terms in the momentum equations, Eqn 5, become non-zero as seen in Eqn 10, where the *i* index indicates the three normal coordinates *x*, *y* and *z*, with *x* and *y* defining the horizontal plane and *z* the vertical. Without the terminal velocity assumption, the time dependence of the mass and velocity of the firebrand is essential for the estimation of the firebrand velocity (*V*):

$$\frac{d}{dt}(mV) = \sum_i \mathbf{F}_i \neq 0 \qquad (10)$$

Discarding the terminal velocity assumption means that the relative wind vector and the firebrand velocity vector are no longer co-planar on the *x*′–*z* plane. This is because the firebrand may have a velocity component perpendicular to this plane, as the direction of relative wind velocity could be changed from an earlier moment. Thus the firebrand could be said to have a decaying memory of previous wind fields it has experienced. Over an extended time of exposure to a wind field with only *x*′–*z* components, any perpendicular velocities will diminish and the firebrand will approach terminal velocity. As shown in Fig. 4*a*, the firebrand's orientation is assumed to be normal to the relative wind on the horizontal plane because a firebrand is

assumed to have no side-lift force and wobbling and tumbling are still being ignored. The implicit assumption that occurs with this treatment is that the orientation of the firebrand reacts in shorter time scales than the changes in wind direction.

Without the terminal velocity approximation, the angle between the relative wind velocity and the static reference horizontal *x*-axis (*β*) is defined in Eqn 11. Note the four expressions in Eqn 11 have the same value, zero, under the terminal velocity assumption. The expressions in terms of *U* and *V* are included in order to remind the reader that without the terminal velocity approximation, the orientation of (*W*), the relative velocity of the wind with respect to the firebrand, is usually not the same as the direction of the local wind velocity (*U*) or the firebrand velocity (*V*).

$$\beta \equiv \tan^{-1}\left(\frac{W_y}{W_x}\right) \neq \tan^{-1}\left(\frac{U_y}{U_x}\right) \neq \tan^{-1}\left(\frac{V_y}{V_x}\right) \qquad (11)$$

In the horizontal plane, the principal directions of the relative wind, *x*′ and *y*′, are defined by the angle of *β*, as seen in Fig. 4. The relative wind velocities in the principal directions are:

$$W_{x'} = U_{x'} - V_{x'} = \sqrt{W_x^2 - W_y^2} \qquad (12a)$$

$$W_{y'} = U_{y'} - V_{y'} = 0 \qquad (12b)$$

Note that:

$$\cos\beta = \frac{W_x}{W_{x'}} = \frac{W_x}{\sqrt{W_x^2 - W_y^2}} \qquad (13a)$$

$$\sin\beta = \frac{W_y}{W_{x'}} = \frac{W_y}{\sqrt{W_x^2 - W_y^2}} \qquad (13b)$$

The forces acting on a firebrand in Eqns 1, 2, 3 and 4 are actually in the vertical direction *z* and the principal direction *x*′, as shown in Fig. 4*b*. The angle of attack between the relative wind vector and the plane containing the disc or the axis of the cylinder is defined by *α*. Thus, the momentum equation found in Eqn 10 can be written in the three axes (*x*, *y* and *z*) as follows:

$$\frac{d(mV_x)}{dt} = \sum F_x$$

$$m\frac{dV_x}{dt} + V_x\frac{dm}{dt} = F_{D,x} + F_{L,x}$$

$$= (F_{D,x'} + F_{L,x'})\cos\beta$$

$$= \frac{1}{2}A_c\rho_a|\mathbf{W}|C_N(W_{x'}\sin\alpha - W_z\cos\alpha)\cos\beta$$

$$= \frac{1}{2}A_c\rho_a|\mathbf{W}|C_N(W_x\sin\alpha - W_z\cos\alpha\cos\beta)$$

$$= \frac{1}{2}A_c\rho_a|\mathbf{W}|C_N W_x$$

$$\times \left(\sin\alpha - \frac{W_z}{\sqrt{W_x^2 + W_y^2}}\cos\alpha\right) \qquad (14)$$

$$\frac{d(mV_y)}{dt} = \sum F_y$$

$$m\frac{dV_y}{dt} + V_y\frac{dm}{dt} = F_{D,y} + F_{L,y}$$

$$= (F_{D,x'} + F_{L,x'})\sin\beta$$

$$= \frac{1}{2}A_c\rho_a|\boldsymbol{W}|C_N(W_{x'}\sin\alpha - W_z\cos\alpha)\sin\beta$$

$$= \frac{1}{2}A_c\rho_a|\boldsymbol{W}|C_N(W_y\sin\alpha - W_z\cos\alpha\sin\beta)$$

$$= \frac{1}{2}A_c\rho_a|\boldsymbol{W}|C_N W_y$$

$$\times\left(\sin\alpha - \frac{W_z}{\sqrt{W_x^2 + W_y^2}}\cos\alpha\right)$$

$$\tag{15}$$

$$\frac{d(mV_z)}{dt} = \sum F_z$$

$$m\frac{dV_z}{dt} + V_z\frac{dm}{dt} = F_{D,z} + F_{L,z} + F_{g,z}$$

$$= \frac{1}{2}A_c\rho_a|\boldsymbol{W}|C_N(W_z\sin\alpha - W_{x'}\cos\alpha) - mg$$

$$= \frac{1}{2}A_c\rho_a|\boldsymbol{W}|C_N$$

$$\times(W_z\sin\alpha - \sqrt{W_x^2 + W_y^2}\cdot\cos\alpha) - mg$$

$$\tag{16}$$

With the terminal velocity assumption, the firebrand orientation is normal to the firebrand velocity and the absolute wind velocity because the directions of the absolute wind vector ($\boldsymbol{U}$), the firebrand velocity vector ($\boldsymbol{V}$) and the relative wind vector ($\boldsymbol{W}$) are in the same plane. However, without the terminal velocity assumption, these vectors have different directions even with no side-lift force assumption.

As dm/dt can be obtained from combustion models and dV/dt can be discretised in time as $(\boldsymbol{V} - \boldsymbol{V}^o)/\Delta t$, if the angle of attack and firebrand velocity of the previous time step ($\boldsymbol{V}^o$) are known, then Eqns 14, 15 and 16 are three independent equations with three unknowns. The unknowns are the three components of the firebrand velocity vector. Therefore, the firebrand velocity can be calculated without the terminal velocity assumption.

Combustion and mass loss models

The combustion process changes firebrands' shapes and densities, which are parameters that affect firebrand dynamics. Tarifa measured combustion effects on firebrand dynamics in wind-tunnel experiments, and then used these data in the trajectory calculations (Tarifa *et al.* 1965a, 1967). Muraszew did similar experiments but focussed on density changes rather than shape changes (Muraszew and Fedele 1976). The current study makes the simplifying assumption that lofted firebrands are already dried out and charred, and so do not change in density while in flight. The density of charred wood, $300\,\text{kg m}^{-3}$, is assumed throughout the firebrand trajectory discussions that follow. This is close to the density of the actual firebrand shown in Fig. 1.

For the current study, the wood is also assumed to be a homogeneous solid, and the mass loss is assumed to be uniform on any burning surface, so that it decreases the height or radius of the disc or cylinder. This is not how firebrands actually burn, because woody material is heterogeneous and is not isotropic. In addition, wood is pyrolysed by heat supplied by heterogeneous (glowing) combustion of the wood on the outer surface of the firebrand or by the diffusion flame enveloping the firebrand (Albini 1979). The pyrolysis of a solid is a surface or volumetric chemical process (Tse and Fernandez-Pello 1998), but these pyrolysed volatiles tend to flow along the grain, so the regression tends to happen along the grain orientation. Thus, real firebrands tend to lose mass in the direction of the grain more easily than in the direction perpendicular to grains, as in typical solid-wood burning processes (Drysdale 1999). However, as Tse and Fernandez-Pello (1998) noted, combustion modelling is difficult without the assumption of uniform regression.

In order to investigate the effect of combustion and resulting mass loss on firebrand transport, firebrands are assumed to be in flaming combustion, which has a greater regression rate than glowing combustion. Even though firebrands in wildfires are more likely in glowing combustion, it has been found that the firebrands in flaming combustion are more effective in igniting recipient fuel beds (Manzello *et al.* 2006a, 2006b). In fact, firebrands may experience transition between flaming to glowing or glowing to flaming combustion, depending on environmental conditions such as oxygen supply and ambient temperature. The modelling of glowing combustion and transition should be studied for more accurate simulation; however, various types of firebrands undergoing flaming combustion are modelled for this study as a first approximation. This is because computational efficiency limits the simulations used in this study to a domain length scale that is less than 1 km, and a simulated duration of less than 200 s, which is too small to see the effect of glowing combustion on firebrand transport, owing to its lower regression rate. It has been found from preliminary study that the transport of glowing-combustion firebrands is not significantly different from the transport of inert particles of the same initial size. However, simulations of firebrands with glowing combustion should be performed in the future, when larger-domain simulations for longer duration are available with reasonable efficiency.

For the combustion and mass loss model in this study, diffusion flame analyses are used to determine the regression rates. Boundary layer diffusion flame analyses are used for cylindrical and disc firebrands, whereas the droplet-burning law was used in previous work for spherical firebrands (Fernandez-Pello 1982; Woycheese *et al.* 1999; Turns 2000; Woycheese 2000). The development of the boundary layer diffusion flame analysis relies on Pagni's classic diffusion flame analyses (Pagni 1981) to obtain mass fluxes at the fuel surface, which are equivalent to the mass loss rates from the firebrand. They are found as functions of the Reynolds number (Re) based on the relative wind speed ($\boldsymbol{W}$) and the firebrand's size; Spalding's mass transfer number (B) (Spalding 1953); and the mass consumption number (γ). B and γ are defined as in Pagni (1981):

$$B \equiv \frac{QY_{o,\infty}/v_o M_o - h_w}{L}, \qquad \gamma \equiv \frac{Y_{o,\infty}v_f M_f}{Y_{f,w}v_o M_o} \tag{17}$$

where Y denotes the mass fraction, v denotes the stoichiometric coefficient, M denotes the molecular weight, Q is the energy released by the combustion of v_f moles of gas phase fuel, h_w is the specific enthalpy at the fuel surface and L is the effective latent heat of pyrolysis. For subscripts, o is oxygen, f is fuel, w is the value at the fuel surface (or wall) and ∞ is a value far from the fuel surface. Using the stoichiometric ratio (s), which is $(v_f M_f)/(v_O M_O)$, and rearranging variables, the mass consumption number can be denoted as:

$$\gamma = \frac{sY_{o,\infty}}{Y_{f,w}}, \qquad \text{where } Y_{f,w} = \frac{BY_{f,t} - sY_{o,\infty}}{1 + B} \quad (18)$$

Here, $Y_{f,t}$ is the fuel mass fraction of the transferred material and is approximated as 1. This quantity accounts for any inert substances in the pyrolysates. This assumes that the Lewis number (Le) is equal to 1, which means that the mass diffusivity equals the heat diffusivity. The mass fraction of fuel at the wall ($Y_{f,w}$) was obtained from mass and energy balances at the fuel surface:

$$\frac{QY_{o,\infty}/v_o M_o - h_w}{L} = B = \frac{Y_{f,w} + sY_{o,\infty}}{Y_{f,t} - Y_{f,w}} \quad (19)$$

As $Y_{o,\infty}$, $Y_{f,t}$, s and B are all approximately constant and known for a given fuel, $Y_{f,w}$ and γ can be calculated as approximately constant for a given fuel material. For this study, B and γ are assumed to be 1.2 and 0.50 for wood firebrands (Woycheese 2000).

Disc and cylindrical firebrands – two limiting cases for combustion mass loss

The mass loss of disc and cylindrical firebrands in reality occurs through regression in both the radial and axial directions. To study the effect of the assumption of uniform regression in either of these directions, two limiting cases are studied: regression only in the axial direction and regression only in the radial direction.

As the gravitational, drag and lift forces of a disc firebrand all linearly depend on radius, the radius term cancels out of the force balance shown in Eqn 7. The relative velocity of a disc firebrand is therefore not a function of its radius. And similarly, the thickness term cancels out of the force balance on a cylindrical firebrand, so its relative velocity does not depend on length, as shown in Eqn 8. If C_N is assumed not to be strongly affected by the change in the h to r ratio for these cases, drag and lift forces will remain at their initial, maximum level throughout the firebrand's flight. The radial regression of disc firebrands and axial regression of cylinder firebrands, then, are one extreme where regression has minimal effects on dynamics. The trajectories of these kinds of firebrands are similar to non-burning firebrands studied by Himoto and Tanaka (2005). However, combustion-driven regression has a maximum effect on dynamics for the other extremes of axial regression of disc firebrands or radial regression of cylindrical firebrands, because all regression occurs in the direction that affects lift and drag forces. Although the latter case appears to be more common, real firebrands may be expected to behave somewhere between these two extremes.
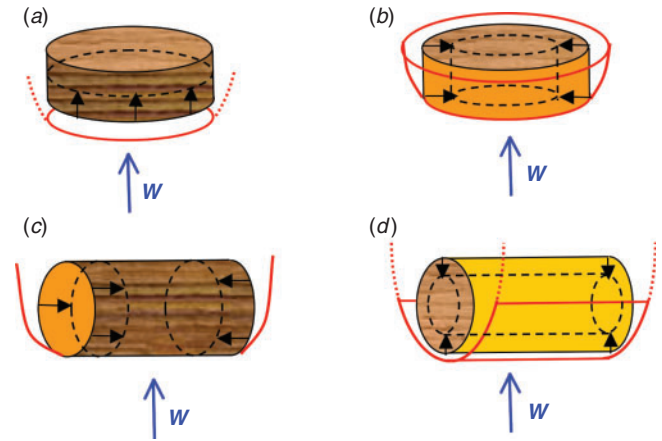

Fig. 5. Four combustion models for discs and cylinders: (*a*) a disc with axial regression (DISC_*dh/dt*); (*b*) a disc with radial regression (DISC_*dr/dt*); (*c*) a cylinder with axial regression (CYL_*dh/dt*); and (*d*) a cylinder with radial regression (CYL_*dr/dt*). Red solid lines indicate the flame sheet in the boundary layer, and the red dotted line indicates possible flames that are ignored in the model. The black arrows indicate the regression direction, the black dotted lines indicate the shape of the firebrand after uniform regression, and the orange and yellow surfaces are the burning regions. For each of these cases, $\alpha = 90°$.

The four combustion models adapted to this study are illustrated in Fig. 5. In the images in Fig. 5, the angles of attack are set to 90°, the position of maximum drag. Boundary-layer diffusion flames are formed around the burning surface in each case. A combusting stagnation-point boundary layer of uniform thickness is formed in the case of disc firebrands with axial regression, shown in Fig. 5*a*. Combusting boundary layers similar to the boundary layer for parallel flow over a flat plate (Emmons 1956) are formed in the other three cases, shown in Fig. 5*b*, *c* and *d*. As a first approximation, the combustion process is averaged over the burning surface so that the radius or thickness is uniformly regressed, and the firebrands retain their shape. Below, the various mass-loss or mass-regression models are described for the axial and radial regression of discs and cylinders.

Opposed flow diffusion flame – disc with axial regression (DISC_dh/dt)

A disc firebrand with axial regression (DISC_*dh/dt*) is shown in Fig. 5*a*. This pattern of mass loss is treated in this text as a limiting case where regression due to combustion has a maximum effect on firebrand dynamics for this shape. Woycheese (2000) modelled the stagnation burning on the windward side of the disc by applying the results of opposed flow diffusion flames analysis (Kinoshita *et al.* 1981) along with dimensional analysis to burning firebrands studied in his wind-tunnel experiments. From a mass flux balance between fuel and oxidiser (air), the mass flux of wood (Kinoshita *et al.* 1981) was found to be:

$$\dot{m}'' = \rho_s \frac{dh}{dt} = 2\rho_a \left(\frac{v|W|}{r}\right)^{1/2} f(0) = 2\rho_a \text{Re}_r^{-1/2}|W|f(0) \quad (20)$$

In this equation, r is the radial coordinate on the disc surface, W is the relative wind velocity, v is the kinematic viscosity of air, h is the firebrand thickness and $f(0)$ is a dimensionless stream function on the surface, which was found through curve-fitting to be:

$$f(0) = -0.353\gamma^{-0.02}B^{0.611-0.651\ln(B)} \tag{21}$$

In Eqn 21, γ is the mass consumption number and B is Spalding's mass transfer number. When B and γ are specified to be 1.2 and 0.50, $f(0)$ is approximately -0.4. To convert this uneven regression rate to a uniform rate across the burning surface with homogeneous mass loss, assuming constant density, the regression rate is averaged as:

$$\left.\overline{\frac{dh}{dt}}\right|_{disc} = \frac{1}{\rho_s \pi r_o^2} \int_0^{r_o} \left(2\rho_a \left(\frac{v|W|}{r} \right)^{1/2} f(0) \right) \cdot 2\pi r dr$$
$$= \frac{8}{3} \frac{\rho_a}{\rho_s} \mathrm{Re}_{r_o}^{-1/2} |W| f(0) \tag{22}$$

where r_o is the current maximum radius of the disc firebrand and $f(0)$ is given by Eqn 21.

Forced boundary layer diffusion flame – disc with radial regression and cylinders

Whereas a stagnation boundary layer is formed on a falling disc firebrand with axial regression, the other cases shown in Fig. 5*b*, *c* and *d* for discs with radial regression (DISC_*dr/dt*) and both cases for cylinders (CYL_*dh/dt* and CYL_*dr/dt*) develop forced flow boundary layers similar to those formed in film combustion of liquid fuel as Emmons (1956) analysed. Pagni (1981) further developed the film combustion model and solved for the mass flux per unit area as:

$$\dot{m}'' = \rho_s \frac{dx}{dt} = \frac{1}{2}\rho_a \mathrm{Re}_x^{-1/2} |W| f(0) \tag{23}$$

where x is the coordinate in the wind direction, W is the relative wind speed and $f(0)$ is a dimensionless stream function. The dimensionless stream function for this case is evaluated at the firebrand surface under the assumption that the Prantl number (Pr) is $= 0.73$, which is true of air (Pagni 1981), through curve-fitting:

$$f(0) = -0.47B^{0.578-0.097\ln B} \tag{24}$$

Because B is taken to be 1.2, $f(0)$ is calculated to be -0.52. These three cases will have different flame shapes on their combusting surfaces, but their boundary layers are all approximated to be the same as the film combustion case. The mass flux defined by Eqn 23 is applied to all three of the cases. The mass flux is then averaged over the entire combusting surface to derive a uniform regression rate, as was done in Eqn 22.

For the radial regression of the disc firebrand shown in Fig. 5*b*, which can be described as edge burning, the total combusting area is $2\pi r h_o$, where h_o is the approximately

constant disc thickness, h is in the axial direction and $dA = 2\pi r dh$. Using Eqn 23, the average regression is then:

$$\left.\overline{\frac{dr}{dt}}\right|_{disc} = \frac{1}{2\rho_s \pi r h_o} \int_0^{h_o} \left(\frac{1}{2}\rho_a \left(\frac{v|W|}{h} \right)^{1/2} f(0) \right) \cdot 2\pi r dh$$
$$= \frac{\rho_a}{\rho_s} \mathrm{Re}_{h_o}^{-1/2} |W| f(0) \tag{25}$$

The regression rates for the cylinder cases are derived similarly. For axial regression, as shown in Fig. 5*c*, both ends of the cylinder are assumed to be burning. Each end has a combusting area of πr_o^2, where r_o is the cylinder radius, r' is parallel to the end surfaces and $dA = 2(r_o^2 - r^2)^{1/2}dr$. Thus, based on Eqn 23, the average axial regression rate assuming both ends are burning is given by:

$$\left.\overline{\frac{dh}{dt}}\right|_{disc} = \frac{2}{\rho_s \pi r_o^2} \int_{-r_o}^{r_o} \left(\frac{1}{2}\rho_a \left(\frac{v|W|}{r} \right)^{1/2} f(0) \right)$$
$$\times 2\sqrt{r_o^2 - r^2}\, dr = 1.11\frac{\rho_a}{\rho_s} \mathrm{Re}_{r_o}^{-1/2} |W| f(0) \tag{26}$$

For radial regression of a cylinder, as illustrated in Fig. 5*d*, the total combusting area is half of the surface area (ignoring end areas), $\pi r h_o$, because only the windward side of the cylinder is assumed to be burning. c runs along the curved surface of the cylinder at a distance r from the centre axis and $dA = h_o dc$. Although only half of the face is burning, the cylindrical shape is assumed to be preserved, so it is as though the cylinder is rotating about its axis, such that uniform regression occurs over the entire surface. Thus, using Eqn 23, the average radial regression rate is:

$$\left.\overline{\frac{dr}{dt}}\right|_{cyl} = \frac{2}{\rho_s \pi r h_o} \int_0^{\frac{\pi r}{2}} \left(\frac{1}{2}\rho_a \left(\frac{v|W|}{c} \right)^{1/2} f(0) \right) \cdot h_o dc$$
$$= \sqrt{\frac{1}{\pi}} \frac{\rho_a}{\rho_s} \mathrm{Re}_r^{-1/2} |W| f(0) \tag{27}$$

Note that the length scale for the Reynolds number in this case is the radius, so the regression rate approaches infinity as r approaches zero. This singularity is avoided by setting a minimum r value below, which the firebrand is assumed to be burned out or to have no effect. In the simulations, this burned-out criterion is set as small as 0.02 mm because even very small firebrands can ignite spot fires in an extreme combination of conditions, such as very fine recipient fuels in high atmospheric temperatures with low relative humidity.

Each of the regression rates derived above, Eqn 22 and Eqns 25, 26 and 27 can be non-dimensionalised by dividing by $(\rho_a/\rho_s)\mathrm{Re}^{-1/2}|W|$. This non-dimensional quantity, defined by Eqn 28, is a function of $f(0)$ alone, which is in turn only a function of B or, for the disc with axial regression, a function of B and γ.

$$\overline{\frac{[dr \text{ or } dh]}{dt}} \bigg/ \frac{\rho_a |W|}{\rho_s \mathrm{Re}^{1/2}} \tag{28}$$
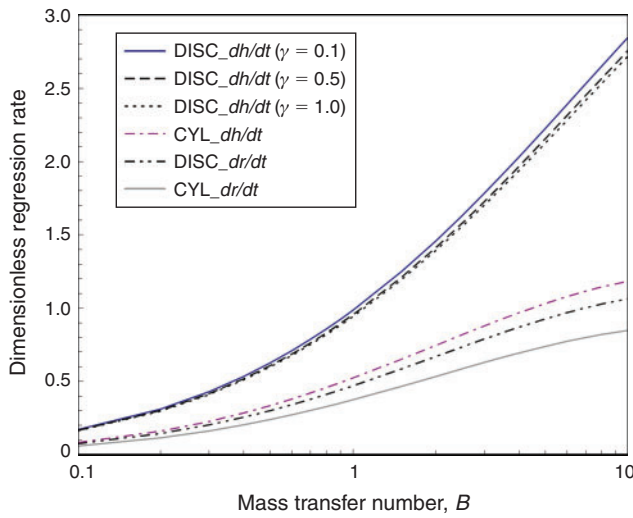
Fig. 6. Dimensionless regression rates for the four combustion models shown as functions of the mass transfer number (B). Only the axial regression rate of the disc firebrand is a weak function of mass consumption number (γ) whereas others are independent of γ. Dimensionless regression rates are defined as $\frac{\overline{dh}}{dt}\left(\frac{\rho_s}{\rho_a}\right)\mathrm{Re}_{r_o}^{1/2}|W|^{-1}$ for disc and cylinder with axial regression, $\frac{\overline{dr}}{dt}\left(\frac{\rho_s}{\rho_a}\right)\mathrm{Re}_{h_o}^{1/2}|W|^{-1}$ for disc with radial regression and $\frac{\overline{dr}}{dt}\left(\frac{\rho_s}{\rho_a}\right)\mathrm{Re}_r^{1/2}|W|^{-1}$ for cylinder with radial regression.

Fig. 6 shows the dimensionless regression rates for the four combustion models, as a function of B. In this study, B is assumed to be 1.2 for wood.

Simulations

Firebrand transport in wildfires was studied by incorporating the models described above into the HIGRAD/FIRETEC wildfire model. HIGRAD/FIRETEC is a multiphase transport model based on ensemble-averaged conservation equations for mass, momentum, energy and chemical species. HIGRAD/FIRETEC couples models for the macroscale effects of processes such as combustion, radiation, convective heat exchange and aerodynamic drag in order to achieve a self-determining coupled atmosphere–fire model. The hydrodynamic aspects of HIGRAD/FIRETEC utilise the method of averages (MOA) approach (Reisner *et al.* 1998, 2000). The physical and chemical formulations of the FIRETEC model are described in detail by Linn (1997) and including recent modifications (Linn *et al.* 2002, 2005; Linn and Cunningham 2005). All of the HIGRAD/ FIRETEC simulations used for the present study have a uniform horizontal grid spacing of 2 m. The vertical grid spacing is stretched with height, with a spacing near the ground of ~1.5 m increasing to ~30 m at the top of the domain at $z = 615$ m. Thus, $320 \times 160 \times 41$ cells are used for the $640 \times 320 \times 615$-m domain. In HIGRAD/FIRETEC, fuels are modelled as porous media. In the simulations for this work, surface fuels were specified with properties similar to tall grass or short chaparral, with a 0.7-m height and surface fuel loading of 0.7 kg m^{-2}. The bulk density within the fuel bed, which is defined as fuel particle mass divided by total fuel cell volume, is 1.0 kg m^{-3}. Though HIGRAD/FIRETEC is capable of modelling heterogeneous fuel beds (Linn *et al.* 2005), which would be more realistic, homogeneous fuel beds are used to eliminate effects of fuel heterogeneity on firebrand launching and transport. In the simulations with canopies, the bulk density within the canopy fuel layer between 3.05 and 19.3 m from the ground is 0.25 kg m^{-3}. Simulated fires are initiated as line fires that are 100 m long and 2 m wide. After ignition, the simulated fires spread for 170 s. For the canopy fuel cases, it is assumed that the transition to crown fire has been completed at the start of the simulations to separate the effects of transition on firebrand transport.

As this study is focussed on the transport of firebrands, ignition by firebrands is not considered. Conservative assumptions are used for firebrand generation, and firebrands are assumed to be produced from loose or degrading fuels during combustion. Thus, the fuel bulk density and the temperature are considered as the criteria for firebrand generation: the FIRETEC computational cells with bulk density higher than 0.01 kg m^{-3} and solid temperature higher than 600 K are considered to be cells that can produce firebrands. Launching positions within the firebrand-producing cell are randomly chosen. As little information is known about how to properly model firebrand generation rates, firebrands are created with arbitrary rates. Ten firebrands per computational cell ($2 \times 2 \times 1.5$ m near the ground) are produced every second for surface fire simulations. Five firebrands per cell per second are generated for crown fires simulations to avoid generating too many firebrands, because crown fires have deeper fuels to generate firebrands. These firebrand generation rates were selected to overcome randomness of firebrand initial positions considering computational efficiency and tested through repeated simulations. Up to ~200 000 firebrands are simulated in each simulation presented here.

The size of the firebrands launched from each cell is taken to be the largest loftable size for that location at that point in time. This approach is based on a large number of simulations in which a range of firebrand sizes were launched. The results showed that the longest trajectories were produced by the larger firebrands because smaller firebrands burn out before they reach the ground at long distances. Aerodynamic drag and lift forces induced by local winds are responsible for firebrand transport. The maximum size of a lofting firebrand is determined by the local vertical wind speed. In order to capture the most hazardous firebrands in simulations, the initial firebrand size is assumed to be the maximum loftable size, which is determined by the upward wind at the initial firebrand location. The initial thickness for discs and the initial radius for cylinders are determined as shown in Eqns 29 and 30.

$$h_{\max,disc} = \frac{1}{2g}\frac{\rho_a}{\rho_s}C_N|\boldsymbol{U}|(U_z\sin\alpha + U_z\cos\alpha) \qquad (29)$$

$$r_{\max,cyl} = \frac{1}{\pi g}\frac{\rho_a}{\rho_s}C_N|\boldsymbol{U}|(U_z\sin\alpha + U_z\cos\alpha) \qquad (30)$$

$\boldsymbol{U}$ is the absolute wind velocity (and is the same as $\boldsymbol{W}$ initially), h is the thickness, r is the radius, ρ is density, C_N is a normal drag coefficient, α is the angle of attack and g is gravitational acceleration. Subscript a is air, s is solid, x is horizontal direction

Table 2.   Summary of surface fire simulations with various firebrand models

Simulation with and without terminal velocity approximation (TVA)	Number of effective firebrands	Average initial mass (g)	Average travel distance (m)	Average flight time (s)	Maximum initial mass (g)	Maximum travel distance (m)	Maximum flight time (s)
DISC_*dh/dt* with TVA (without TVA)	33 865 (34 621)	0.09 (0.09)	1.7 (6.4)	1.27 (1.84)	0.13 (0.08)	41.0 (50.8)	15.34 (7.34)
DISC_*dr/dt* with TVA (without TVA)	31 762 (32 667)	0.09 (0.09)	1.3 (6.60)	1.05 (1.80)	0.06 (0.14)	10.7 (227.80)	6.66 (26.36)
CYL_*dh/dt* with TVA (without TVA)	14 300 (15 783)	0.003 (0.003)	1.07 (1.79)	0.86 (7.30)	0.003 (0.002)	9.30 (82.30)	2.60 (9.58)
CYL_*dr/dt* with TVA (without TVA)	16 151 (14 580)	0.003 (0.003)	1.27 (7.4)	0.95 (1.77)	0.003 (0.003)	11.8 (26.4)	5.26 (3.30)

of the wind and z is the vertical direction. Another assumption associated with simulating the largest-possible spot fire distance is that the angle of attack is 90°. This assumption allows the maximum drag force on the firebrands and is the most stable condition, as Tarifa observed in his wind-tunnel experiments (Tarifa *et al.* 1965a). In reality, there would certainly be some firebrands that would not have this attack angle; however, smaller angles will result in smaller firebrands being launched. The radius of a disc and the length of a cylinder are not involved in the dynamic models of firebrands because both the gravity force (volume) and the drag force (projected area) are proportional to the radius of a disc or the length of a cylinder. Thus, theoretically, the drag is independent of these values. For the simulations in this study, a fixed aspect ratio was chosen for simplicity, i.e. aspect ratios were fixed as constants: 4.5 for the radius-to-thickness ratio of discs and 6 for the length-to-radius ratio of cylinders. These aspect ratios are based on a firebrand from the Oakland Hills Conflagration (Koo *et al.* 2010) and experimental studies by Tarifa *et al.* (1965a), Muraszew (1974), Muraszew *et al.* (1975), Muraszew and Fedele (1976) and Woycheese (2000, 2001).

Lower limits of initial firebrand sizes to be launched are set to avoid modelling the trajectories of firebrands that will not be effective spotting agents owing to their small size or short transport distances. The cut-off values for thickness of disc firebrands in this study are 1 mm for the surface fires and 5 mm for the crown fires. The radius cut-off values for cylindrical firebrands are 0.75 mm for the surface fires and 3.75 mm for the crown fires. These cut-off values are set based on previous studies that included the optimal firebrand size for maximum travel distance (Koo *et al.* 2007; Koo 2008).

For the purposes of this work, the firebrands have five outcomes: (1) landing within cells containing unburned and unignited fuel; (2) landing on already burned (or burning) cells; (3) staying in the air until the end of the simulation; (4) hitting a boundary of the computational domain; or (5) burning out completely before landing. Because the eventual fate of firebrands that are still aloft at the end of the simulation or that cross the boundary of the computational domain is not known, and firebrands landing in already burning or burned fuels are not going to start new fires, only the firebrands that land on unburned fuel are studied as having the potential to be 'effective'. For each potentially effective firebrand, the initial size of the firebrand and travel distance, as well as the launching and landing locations are recorded and used to generate a variety of distributions for gross firebrand behaviour investigations.

Surface fire simulations

The four models of firebrands with and without terminal velocity approximations were compared in the context of surface fire simulations. Disc and cylindrical models with limiting cases of combustion models were tested. The inlet boundary conditions are sheared-wind profiles using $U_x = 6(z/2.26)^{1/7}$ (one-seventh power law with $6\,\mathrm{m\,s^{-1}}$ at $z = 2.26\,\mathrm{m}$ above the ground), where mid-flame height is assumed. Table 2 shows a summary of the results from eight surface fire simulations with various models and assumptions. The average initial size of effective firebrands is almost the same with the different models: 0.09-g disc with a thickness of 1.65 mm and 0.03-g cylinder with a diameter of 1.64 mm. Note that the sizes of the firebrands, which actually indicate the ability of the fire to loft them, are small because these are surface fires. In surface fires, the fuel bed is very close to the ground, and therefore there is not enough space below the firebrands for the entrained wind to accelerate and launch firebrands. As a result, the vertical velocities at the location where the firebrands are to be launched are fairly small ($\sim 4\,\mathrm{m\,s^{-1}}$). However, the size of the launched firebrands in these simulations are comparable with some types of surface fuel, such as thin bark fragments (Ellis 2000, 2010) for the disc model and pine needles for the cylindrical model.

As shown in Table 2, the models without the terminal velocity assumption are found to travel further because removing the assumption allows the momentum of the firebrands to increase their speed beyond the point where the winds slow down. Note that with the terminal velocity approximation, the horizontal velocity will always be equal to the wind at that location because there is no horizontal body force. In reality and without the terminal velocity approximation, firebrands can fly faster than their immediate-surrounding winds if they carry momentum from stronger winds that they were previously exposed to. This is essentially the notion of a firebrand being thrown by locally strong winds, whereas with the terminal velocity approximation, firebrands cannot be thrown, because it would be similar to throwing a piece of dust. The average travel distances are 1.07 to 1.7 m with the terminal velocity assumption and 6.4 to 7.4 m without the terminal velocity assumption.

As described in the models section, the shape change of firebrands due to combustion can affect their aerodynamics. Combustion affects the trajectories of DISC_*dh/dt* and CYL_*dr/dt*, not DISC_*dr/dt* and CYL_*dh/dt*. The combustion effects made DISC_*dh/dt* and CYL_*dr/dt* travel farther with the terminal velocity assumption. However, the momentum of firebrands
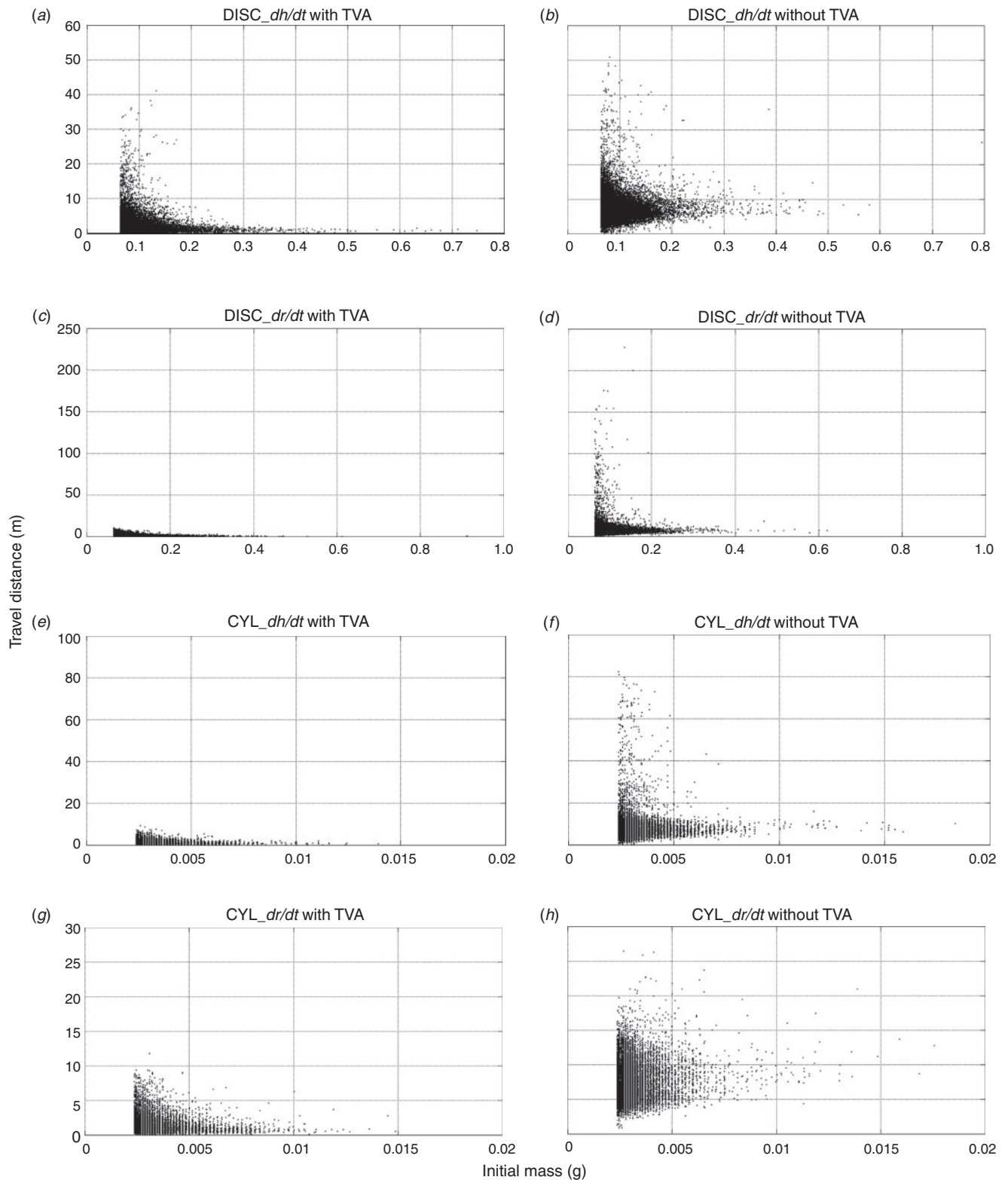
Fig. 7. Travel distance *v*. initial mass of various firebrand models in surface fire simulation with 6-m s^{-1} wind at the mid-flame height: (*a*) DISC_*dh/dt* with terminal velocity approximation (TVA); (*b*) DISC_*dh/dt* without TVA; (*c*) DISC_*dr/dt* with TVA; (*d*) DISC_*dr/dt* without TVA; (*e*) CYL_*dh/dt* with TVA; (*f*) CYL_*dh/dt* without TVA; (*g*) CYL_*dr/dt* with TVA; and (*h*) CYL_*dr/dt* without TVA.

is much more significant than the combustion effect on trajectories. As DISC_*dr/dt* and CYL_*dh/dt* have a smaller burning area, they have a longer lifetime, and it is also possible for them to have greater travel distances. In the cases of DISC_*dh/dt* and CYL_*dr/dt*, the firebrands tend to burn faster and burn out more easily because the area burning is a more significant proportion of the surface area, and so they have shorter travel distances. Fig. 7 shows scatter plots of travel distance *v.* initial mass, in which each dot represents an effective firebrand.

As shown in Fig. 7, eliminating the terminal velocity assumption, which is more realistic with dynamic wind fields, allows circumstances where firebrands can be carried farther. Fig. 8 shows the launching and landing positions of 500 firebrands that travelled farthest for each model. The initial fireline is at $x = -220$ m and is 100 m long. Fig. 9 shows how the fireline spreads over 40-s intervals (Fig. 9*a* at 40 s, Fig. 9*b* at 80 s, Fig. 9*c* at 120 s and Fig. 9*d* at 160 s). As observed in wind-driven surface fire experiments (Fons 1946; Anderson 1983), the fastest spread in the axial direction occurs at the centre of the fireline, which takes on a relatively symmetric crescent shape. Detailed discussions about the shape of the fireline in surface fires is presented in Linn and Cunningham (2005).

The launching and landing locations of the firebrands with longer travel distances are directly related to the buoyant plume structure. It is observed in Fig. 8 that the firebrands having the longest trajectories come from particular regions near the edges and in the centre of the fireline. This trend is illustrated by the fact that there is not an even distribution of grey circles in the burned region and the streaks of launching and landing positions in Fig. 8. The locations of concentrated firebrand launches resulting in long trajectories in the interior of the fireline vary from simulation to simulation. However, in each of the simulations, the combined buoyant force and vertical vortices that occur near the ends of the fireline cause focal points for long-travelling firebrands. As the firelines progress and the shape of the lines becomes more curved, the centre of the fireline, or the apex of the curved fire shape, becomes a focal point for launching firebrands that will travel long distances. These regions of strong buoyant plume are shown in Fig. 9. Further discussion on the effects of plume structure on firebrand transport, which determines launching and landing positions of long-distance firebrands, is presented in the canopy-fire simulation section below.

Crown-fire simulations

The disc and cylindrical firebrand models were simulated in the context of a fire burning in both canopy and surface fuels. Firebrands are modelled without the terminal velocity assumption, because it has been shown that the terminal velocity assumption is not valid with dynamic wind fields from HIGRAD/FIRETEC simulations. The same wind-shear profile used in the surface fuel simulations is used as a boundary condition for the crown fire simulations; however, the drag from the canopy modifies the wind profile during the simulation. The effects of drag from the canopy on wind-shear profiles when using HIGRAD/FIRETEC has been discussed in Pimont *et al.* (2009). The wind speed at the boundary is ~ 9.3 m s^{-1} at 50 m from the ground.
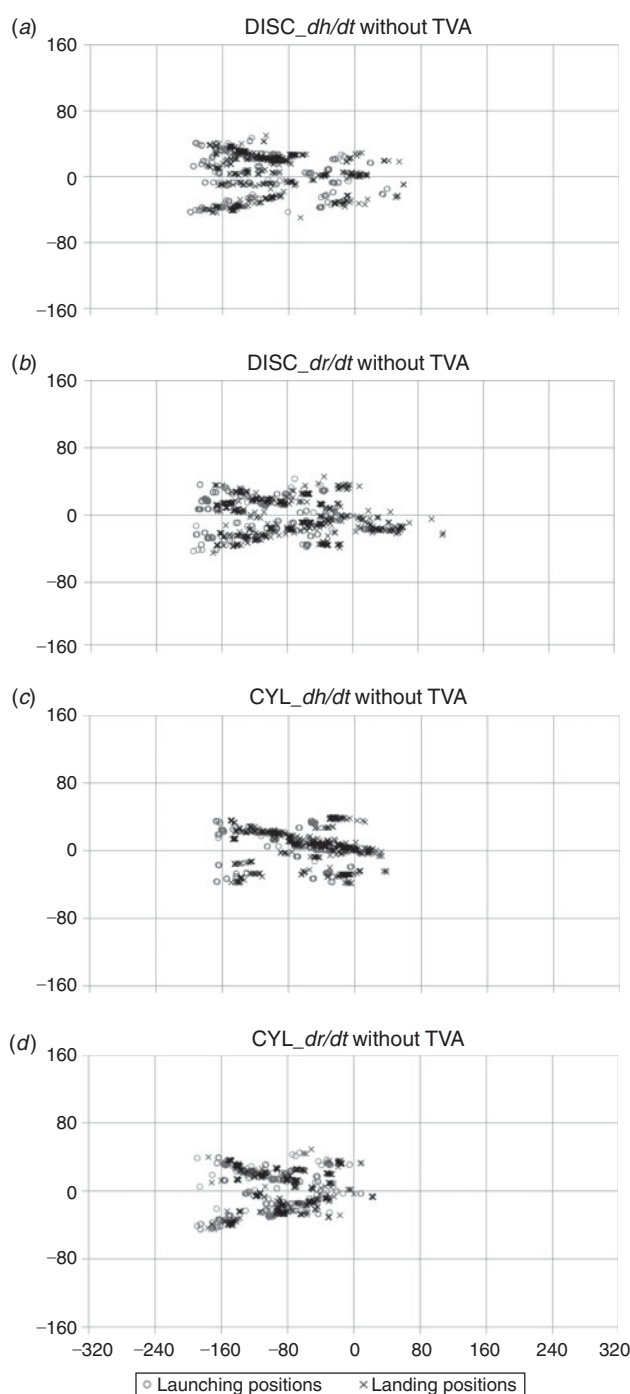

Fig. 8. Launching positions (grey circles) and landing positions (black crosses) of 500 firebrands with the furthest travel distance for various models without terminal velocity assumption in surface fire simulations with a 6-m s^{-1} wind at mid-flame height on the 640×320-m domain: (*a*) DISC_*dh/dt* without TVA; (*b*) DISC_*dr/dt* without TVA; (*c*) CYL_*dh/dt* without TVA; and (*d*) CYL_*dr/dt* without TVA.

Table 3 shows a summary of the results from four firebrand simulations with the crown fire scenario. Crown fires have significantly greater potential to launch firebrands than surface fires: stronger buoyant forces are induced by the fire in the
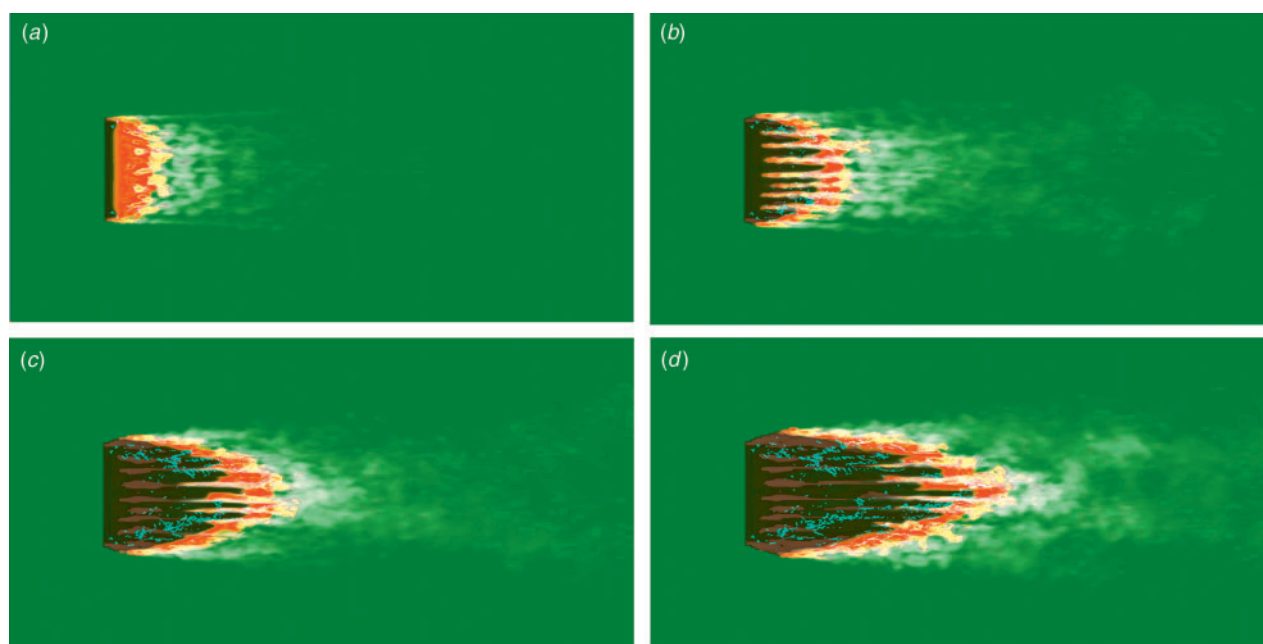
Fig. 9. Top view of surface fire simulations with CYL_*dr*/*dt* models as the fire progresses. The first picture shows 40 s after ignition and time between each frame is 40 s: (*a*) 40 s; (*b*) 80 s; (*c*) 120 s; and (*d*) 160 s after ignition. Turquoise dots indicate where effective firebrands have landed.

Table 3. Summary of crown fire simulation with various firebrand models

Simulation with and without terminal velocity approximation (TVA)	Number of effective firebrands	Average initial mass (g)	Average travel distance (m)	Average flight time (s)	Maximum initial mass (g)	Maximum travel distance (m)	Maximum flight time (s)
DISC_*dh*/*dt*, without TVA	157 343	5.40 (6.32)	73.4	13.71	11.85 (8.03)	502.4	49.14
DISC_*dr*/*dt*, without TVA	205 304	5.01 (6.20)	91.21	14.36	2.46 (5.05)	530.21	54.58
CYL_*dh*/*dt*, without TVA	8335	0.41 (4.15)	88.16	13.42	0.41 (4.16)	516.26	45.28
CYL_*dr*/*dt*, without TVA	4813	0.43 (4.21)	60.66	11.20	1.88 (6.93)	300.01	33.22

deeper fuel bed, and there is more space below the canopy for winds to accelerate upward to the point where the brands are launched. Thus, larger numbers of substantial-sized firebrands are launched from crown fires and transported significant distances. By comparing Table 2 and Table 3, it can be seen that the discrepancy between the number of effective disc firebrands and cylindrical firebrands is larger in the crown-fire simulations than for the surface fire simulations. This is because discs are more aerodynamically responsive to local winds than cylinders owing to the disc's larger drag, and the crown fires have a stronger buoyant plume structure, which contains a wide distribution of vertical velocities.

Note that the disc firebrands represent thin flat firebrands such as those caused by bark flakes (Ellis 2000, 2010) or even those produced by building materials, such as the example in Fig. 1 originating from shake shingles in the Oakland Hills Fire. The firebrands from grasses, twigs or needles can be assumed to have cylindrical shapes, as observed in recent experiments (Manzello *et al.* 2007). The combustion model that is the most realistic for firebrands from forest fires, which would be broken

pieces of tree needles, twigs and branches, should be the radial-direction cylinder regression model (CYL_*dr*/*dt*). The high numbers of effective disc firebrands with significant thicknesses shown in Table 3 indicate that structures in WUI areas could be sources of the more dangerous firebrands. The study of structure fires as a firebrand source should be carried out together with a study of structures as a recipient fuel for firebrands.

Fig. 10 shows travelled distance and initial mass of firebrands in the crown-fire simulations with scatter plots and histograms. Note that the number of effective firebrands indicates the relative potential of firebrand transport for each case, rather than the numbers of actual firebrands that could be produced in each scenario. In the cases where combustion mass loss does not affect the aerodynamics of firebrands, DISC_*dr*/*dt* and CYL_*dh*/*dt*, the most probable travel distance is near zero and the maximum travel distance occurs for brands with minimal mass. The limiting cases where combustion models affect aerodynamics the most, DISC_*dh*/*dt* and CYL_*dr*/*dt*, have maximum travel distances that are shorter than DISC_*dr*/*dt* and CYL_*dh*/*dt*, but these maximum travel distances occur for
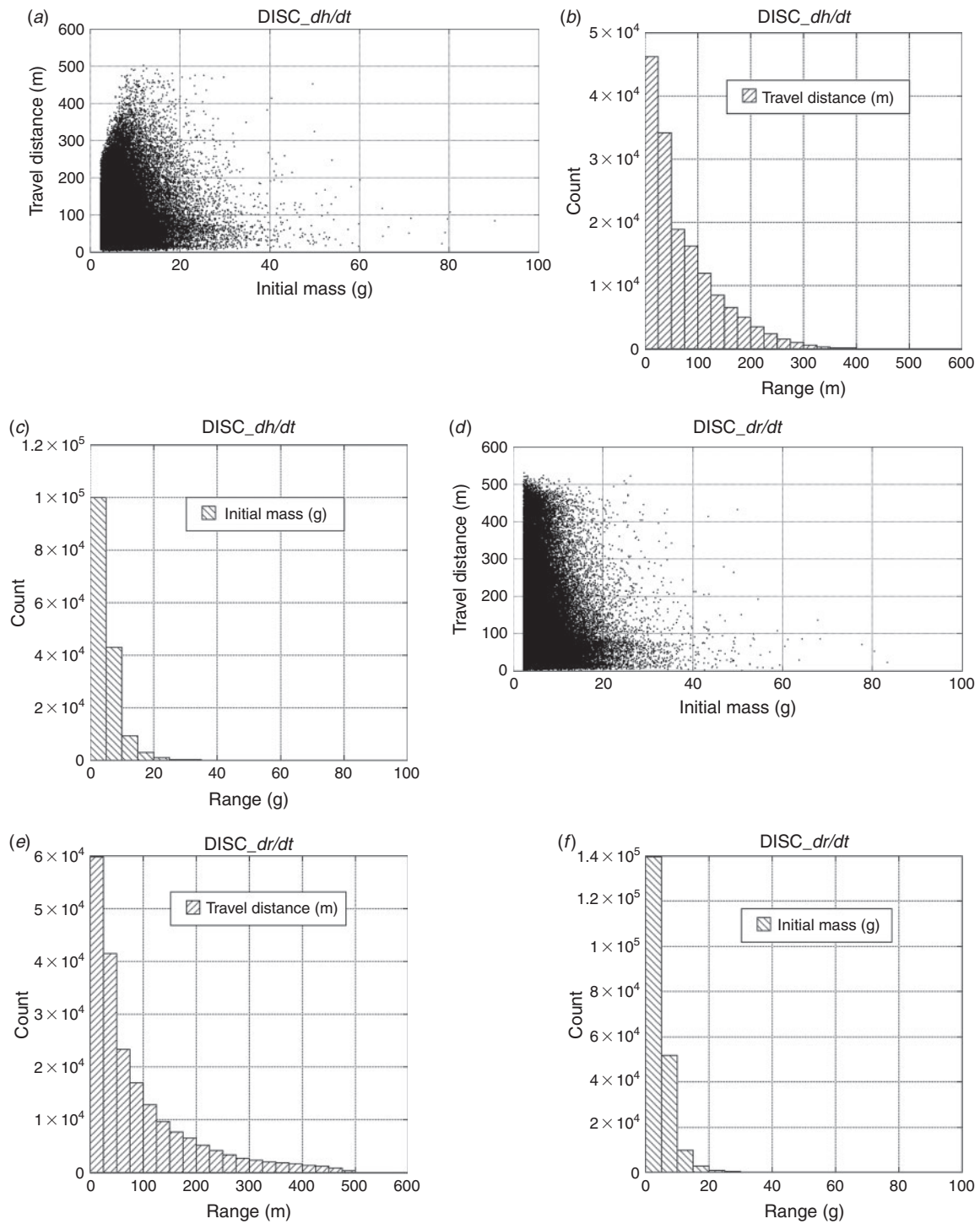
Fig. 10. Travel distance *v.* initial mass of various firebrand models without terminal velocity assumption in canopy fire simulation: DISC_*dh*/*dt* (*a*) scatter plot; (*b*) histogram of travel distance; and (*c*) histogram of initial mass; DISC_*dr*/*dt* (*d*) scatter plot; (*e*) histogram of travel distance; and (*f*) histogram of initial mass; CYL_*dh*/*dt* (*g*) scatter plot; (*h*) histogram of travel distance; and (*i*) histogram of initial mass; CYL_*dr*/*dt* (*j*) scatter plot; (*k*) histogram of travel distance; and (*l*) histogram of initial mass.

firebrands of larger mass than the minimum. These trends are caused by the increase in surface area/weight ratios that occur simultaneously as the firebrands burn at a faster rate than the DISC_*dr*/*dt* and CYL_*dh*/*dt* cases. The smallest firebrands in DISC_*dh*/*dt* and CYL_*dr*/*dt* burn out before they land. This is also related to the lower numbers of effective firebrands in DISC_*dh*/*dt* and CYL_*dr*/*dt* than in DISC_*dr*/*dt* and CYL_*dh*/*dt* in Table 3.
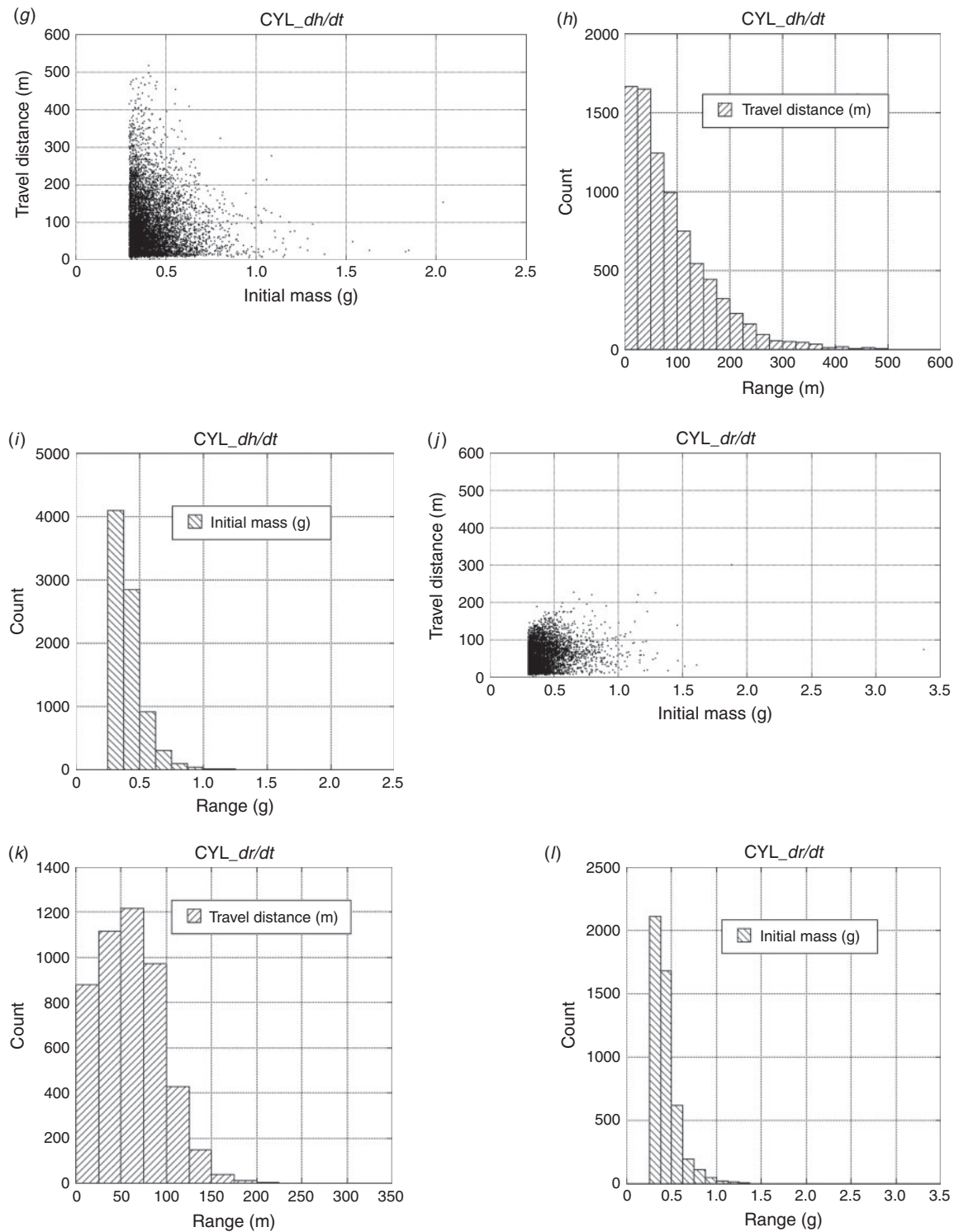
Fig. 10. (*Continued*)

Fig. 11 shows scatter plots of launching and landing positions of simulated effective firebrands in crown fires. Each dot represents an effective firebrand in the simulations. As discussed for surface-fire simulations, plume structure determines where dangerous firebrands are launched and land. As for surface line fire behaviour, strong buoyant vortices develop at the edge of the firelines in all of the simulations. For cylinder simulations, most of the firebrands are launched at the edges, with a few effective firebrands launched at the centre of the fireline. During 170 s of simulated fire spread, the buoyant
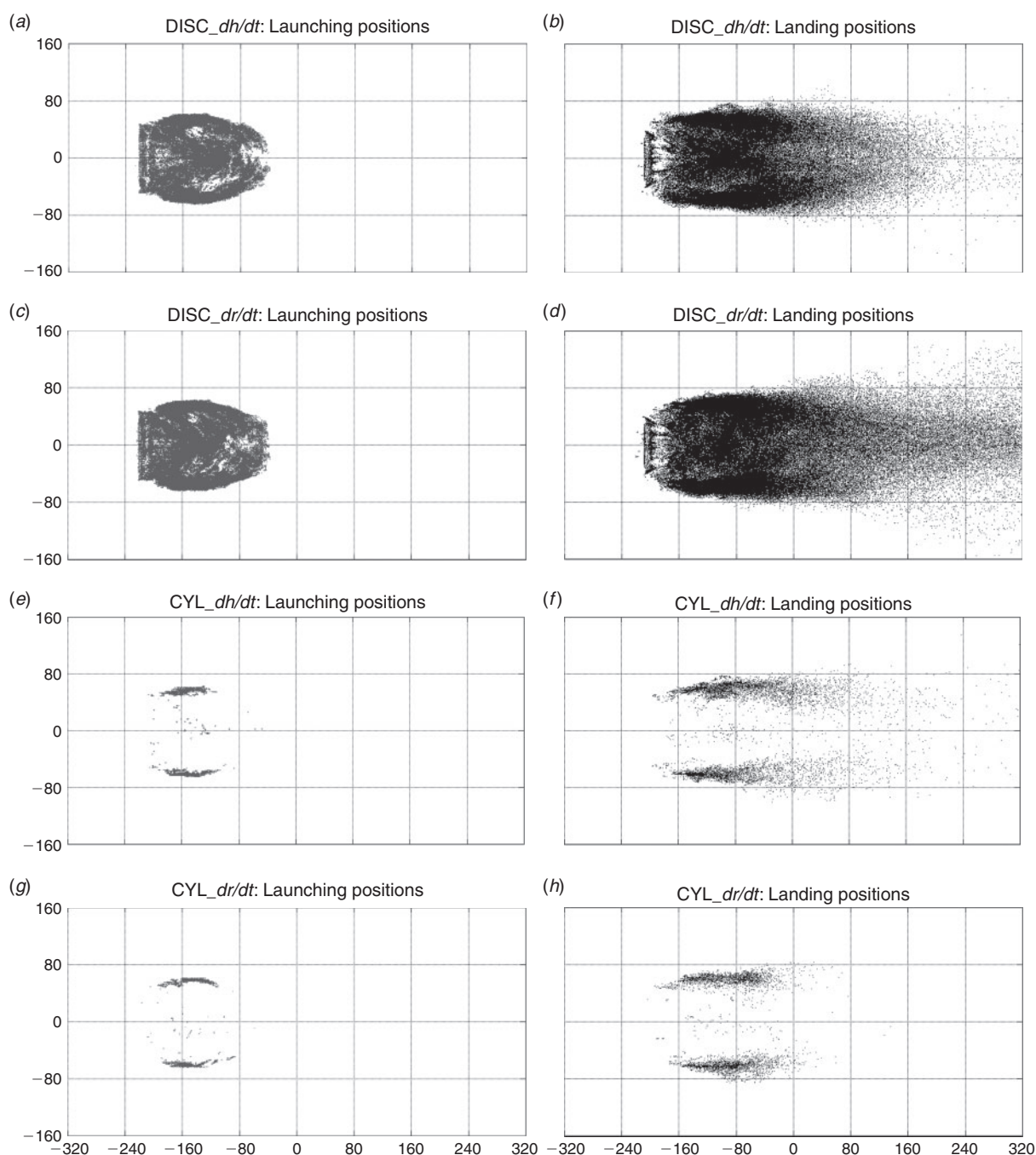
Fig. 11. Launching positions (grey dots in *a*, *c*, *e* and *g*) and landing positions (black dots in *b*, *d*, *f* and *h*) of firebrands in crown fire simulations on the 640 × 320-m domain: DISC_*dh/dt* (*a*) launching positions; (*b*) landing positions; DISC_*dr/dt* (*c*) launching positions; (*d*) landing positions; CYL_*dh/dt* (*e*) launching positions; (*f*) landing positions; CYL_*dr/dt* (*g*) launching positions; (*h*) landing positions.

vortex aided by entrainment at the edge is stronger than at the centre of the fireline. Thus, cylindrical firebrands, which are not as aerodynamically effective as discs, are picked up at the edges but infrequently in the centre. For disc firebrands, which are more easily lofted, launch sites are more widely distributed throughout the moving fire perimeter.

The buoyant updrafts in the interior of the crown fires include stronger vertical winds above the canopy than those of surface fuels, and so they are more effective at entraining disc firebrands throughout the fireline. The disc firebrands, which are lofted higher than cylinders, are trapped deeper within the large buoyant plume and stay longer near the centreline of the plume. For this reason, firebrands with longer travel distances primarily land near the centreline of the domain, as shown in Fig. 12*a*. Fig. 12 shows a scatter plot of travel distance *v*. *y*-direction landing positions and a histogram of the *y*-direction launching
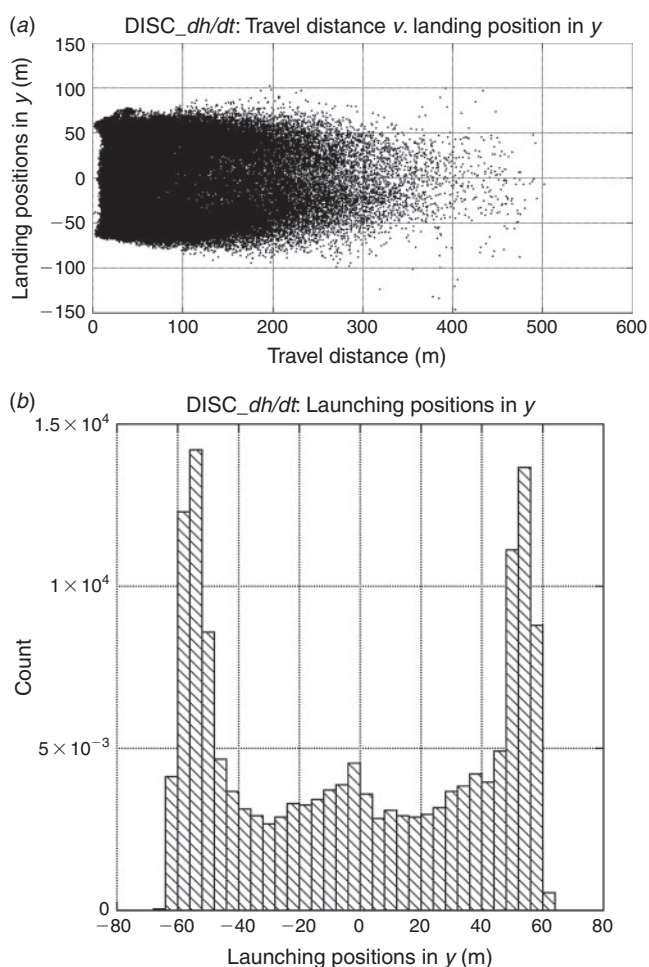
Fig. 12. (*a*) Travel distance *v*. landing positions in the *y* direction: firebrands that travelled further landed near the centreline of the fireline. (*b*) Firebrand launching distributions in the *y* direction: the edges of the fireline launched more firebrands.

positions from the DISC_*dh*/*dt* simulation. Though a higher percentage of the firebrands is launched near the edges of the fireline, as shown in Fig. 12*b*, those not trapped in the centre of the plume tend to be ejected from the plume earlier in their trajectory, and therefore do not travel as far. At the edges, entrainment dilutes the hot gases with cooler air so buoyant forces are damped, whereas hot gases are drawn towards the centre of the fireline to form the most concentrated area of the buoyant plume at the centre of the burning region. If discs are trapped in the central area of the fireline, they can be carried higher than in the vortices at the edges. Visualisations of plume structure are shown in Fig. 13*a* at 40 s, Fig. 13*b* at 80 s, Fig. 13*c* at 120 s and Fig. 13*d* at 160 s after ignition. At 120 s after ignition, shown in Fig. 13*c*, the strong vertical structure at the edges is already formed.

The study of plume structure is crucial for the prediction of firebrand transport and the positions of potential spotting ignitions. The majority of previous studies of firebrand transport focussed on maximum spot fire distance. However, information about locations with a high probability of spot ignition is also

important. For example, firebrands launched at the edge of the fireline could move laterally, as shown in Fig. 11, to initiate or assist the spread of flanking fires. Spotting near the edge of a fireline could cause the escape of a prescribed burn or fire in other wildfire management scenarios.

Conclusions and future works

Firebrand transport is studied with various dynamics and combustion models of disc and cylindrical firebrands by modelling their trajectories within a coupled-physics fire model, HIGRAD/ FIRETEC. Discs and cylinders are assumed to be representative of a wide variety of actual firebrands, and models for these shapes are explored. Based on previous studies and observations, the disc firebrand model is considered to be representative of many firebrands from structures as well as some natural vegetation sources, and cylinders are considered to represent firebrands from twigs, needles and branches. A dynamics model is described for each shape based on the balance between drag, lift and gravitational forces during flight.

For these shapes of firebrands, the implications of the terminal velocity approximation are studied in the context of surface fires. Though the terminal velocity approximation was suitable for simplified wind and plume models, it was found that this assumption has significant effects on firebrand trajectories when applied in the context of non-steady inhomogeneous plumes such as those generated by coupled fire–atmosphere models or real wildfires. The terminal velocity approximation assumes that the firebrand's velocity in the horizontal direction immediately dampens to the velocity of the surrounding wind field, and immediately decelerates in the vertical direction when a firebrand leaves an area of rising air to move into the outside of the plume where the vertical velocity of surrounding air is much smaller. These two implications of the approximation have significant effects when firebrands are travelling in very heterogeneous and transient conditions, and so are not believed to be appropriate for complex physics–fire models. With the dynamic wind fields of HIGRAD/FIRETEC, travel distances simulated using models without the terminal velocity assumption are significantly greater than those obtained with this approximation.

The dynamics models are also paired with combustion models because the shape changes due to the combustion process, defined as regression of mass, affect the firebrand's aerodynamic characteristics. Regression rates are obtained from simple combustion analyses based on forced-convection boundary-layer combustion for cylinders and discs. Two limiting cases of combustion models are developed for discs and cylinders, axial regression and radial regression. Discs with axial regression (DISC_*dh*/*dt*) and cylinders with radial regression (CYL_*dr*/*dt*) are studied as the cases where combustion has the maximum effect on firebrand trajectories. However, discs with radial regression (DISC_*dr*/*dt*) and cylinders with axial regression (CYL_*dh*/*dt*) are the cases where combustion has no effect on firebrand transport, except burnout effects that limit the firebrand's lifetime.

Firebrand trajectory simulations are performed with HIGRAD/FIRETEC modelling a line fire burning in surface fuels and canopy fuels. Eight models (combinations of two
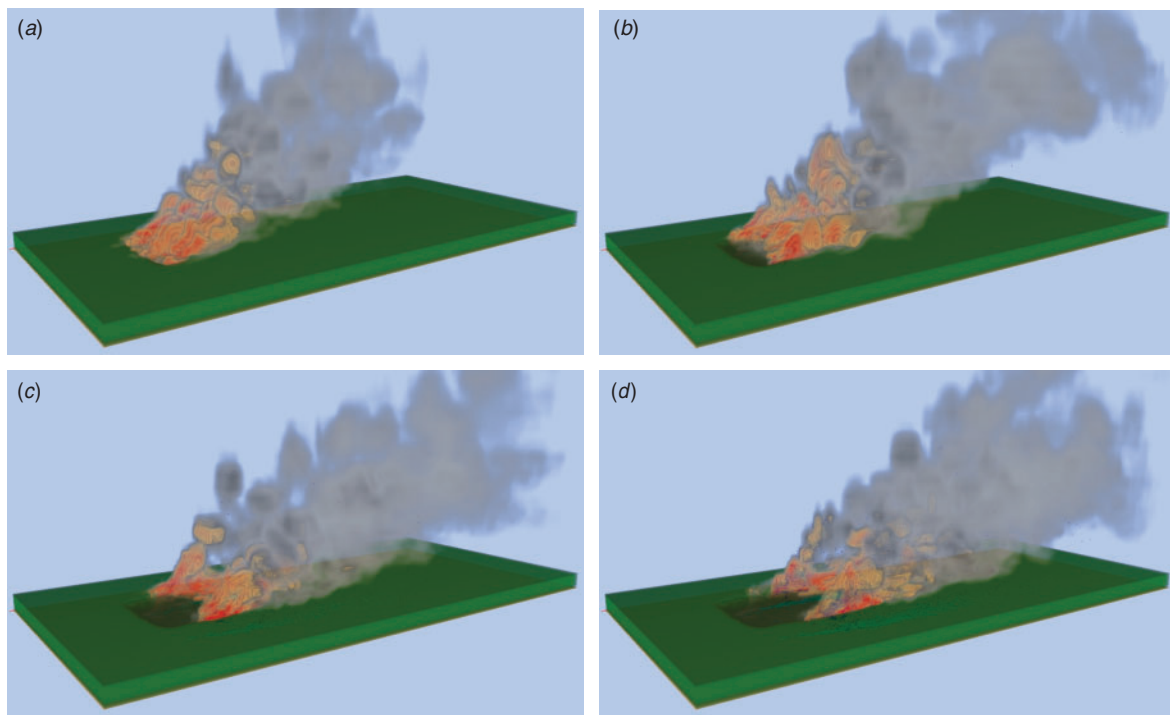
Fig. 13. Crown fire simulation with CYL_*dr*/*dt* with the view from behind as fire progress. The first picture shows 40 s after ignition and time between each frame is 40 s: (*a*) 40 s; (*b*) 80 s; (*c*) 120 s; and (*d*) 160 s. Dark blue dots indicate firebrands in flight and turquoise dots on the ground indicate where effective firebrands have landed.

shapes, two regression directions, and with and without the terminal velocity approximation) of firebrands are simulated with surface fuels and four models (two shapes, two regression directions) are simulated with canopy fuels. Only models without the terminal velocity approximation are applied in the crown-fire case because the terminal velocity assumption was shown to be inappropriate even in the context of the weaker surface-fire simulations. Larger-sized firebrands from canopy fuels travel further than firebrands from surface fires. This is related to the ability of the buoyant updraft to lift canopy fuels as well as the fact that there is more fuel and the fires are more intense. Discs travel further than cylinders, because discs have a larger drag/weight ratio when their attack angle is assumed to be 90°. Discs with axial mass regression and cylinders with radial mass regression are more mobile owing to their increased surface area per weight ratio as they fly, but they have shorter lifetimes owing to their larger burning area. Thus, discs with radial regression travel furthest. Plume structure decides launching and landing positions for firebrands that travel further. In the surface-fire cases studied, line fires on flat terrain, most of the firebrands that travelled the farthest were launched at the edges or centre of the fireline, where the buoyant force is stronger. In the crown-fire cases, the edges of the fireline are able to lift larger firebrands, but the centre is able to transport firebrands further.

There are several critical environmental factors that are expected to couple with fireline behaviour and plume structure to have a significant effect on firebrand transport. The topography of the fire site is crucial, because it determines the shape of

firelines, direction of fire spread, entrainment of air, focus of the updraft, natural wind separation (such as occurs on the lee side of a ridge), or natural impingement of a plume on a hillside (Linn *et al.* 2010). Firebrands from moving fires with non-steady winds (Albini 1982) tend to be retained in the convective column and released during pulses of lower fire intensity, often referred as downdraft, such that a travelling fire may only release firebrands sporadically. Fuel structure is another factor. In addition to the fact that the type of fuel determines the type of firebrands and intensity of the original fire as discussed earlier, the entrainment flow though the fuel bed is strongly affected by its structure. This entrainment directly affects the strength of the vertical velocity at the locations where firebrands are launched (Linn *et al.* 2005). Heterogeneity of fuel and the structure of mixed fuel types could play an important role in determining the entrainment, updraft and flame and plume structures and therefore the firebrand transport. Simulations of HIGRAD/FIRETEC with fuel breaks (Pimont *et al.* 2009) demonstrated that the entrainment flow from the fuel break side was enhanced when the fireline hit the fuel break owing to a decrease in drag. The enhanced entrainment can loft more firebrands, which coincides with the field experiments and observations: a fire that reaches a fuel break often releases a shower of firebrands (Gould *et al.* 2009). In addition to local geophysical factors, atmospheric conditions are critical for the long-range firebrands that reached more than 100 m above the canopy in this study, and sometimes reach over a few kilometres in large conflagrations (Wilson 1962). The plume structure at these altitudes is strongly dependent on the atmospheric events in the planetary boundary layers,

such as the föhn wind (Millán *et al.* 1998), localised sea breezes (Cunningham 2007; Hanley *et al* 2012), upper- and low-level jets (Schaefer 1957; Sharples 2009) and the stability of the boundary layer. These larger-scale phenomena should be studied and incorporated into wildfire research as a factor in plume structure and firebrand transport in large-scale fires. These other environmental factors will be the subject of future work.

Nomenclature

A_c, cross-sectional (projected) area
B, Spalding's mass transfer number, see Eqn 17
C_D, drag coefficient
C_L, lift coefficient
C_N, normal pressure coefficient
CYL_dh/dt, cylinder with axial regression firebrand model
CYL_dr/dt, cylinder with radial regression firebrand model
DISC_dh/dt, disc with axial regression firebrand model
DISC_dr/dt, disc with radial regression firebrand model
F, force
$f(0)$, dimensionless stream function
g, acceleration due to gravity
h, thickness of disc or length of cylinder
h_w, the specific enthalpy at the fuel surface
L, effective latent heat of pyrolysis
Le, Lewis number
M, molecular weight
m, mass
Pr, Prandtl number
Q, energy released by combustion of v_f moles of fuel
r, radius or radial coordinate
Re, Reynolds number
s, stoichiometric ratio, $(v_f M_f)/(v_O M_O)$
U, wind velocity with respect to the ground (absolute velocity)
V, velocity of firebrand with respect to the ground (absolute velocity)
V, volume
W, relative wind velocity with respect to the firebrand
x, y, normal coordinates in the horizontal plane
x', y', principal directions of relative wind in the horizontal plane
Y, mass fraction
z, vertical direction

Greek

α, angle of attack or thermal diffusivity
β, angle between the relative wind velocity and the static reference horizontal x-axis
γ, mass consumption number, see Eqn 18
ρ, density
v, kinematic viscosity or stoichiometric coefficient

Subscripts

90°, 90° of the angle of attack
a, air
cyl, cylinder

disc, disc
D, drag
f, fuel
g, gravity
L, lift
O, oxygen
o, initial value
s, firebrand (solid)
t, transferred gas
w, fuel surface
z, vertical
∞, ambient

Superscripts

o, previous time step

References

Albini FA (1979) Spot fire distance from burning trees: a predictive model. USDA Forest Service, Intermountain Forest and Range Experiment Station, General Technical Report GTR-INT-56. (Ogden, UT)

Albini FA (1981) Spot fire distance from isolated sources: extensions of a predictive model. USDA Forest Service, Intermountain Forest and Range Experiment Station, Research Note RN-INT-309. (Ogden, UT)

Albini FA (1982) Response of free-burning fires to non-steady wind *Combustion Science and Technology* **29**, 225–241. doi:10.1080/00102208208923599

Albini FA (1983*a*) Potential spotting distance from wind-driven surface fires. USDA Forest Service Intermountain Forest and Range Experiment Station, Research Paper RP-INT-309. (Ogden, UT)

Albini FA (1983*b*). Transport of firebrands by line thermals. *Combustion Science and Technology* **32**, 277–288. doi:10.1080/00102208308923662

Anderson HE (1983) Predicting wind-driven wildland fires size and shape. USDA Forest Service, Intermountain Forest and Range Experiment Station, Research Paper INT-305. (Ogden, UT)

Baum HR, McCaffrey BJ (1989) Fire induced flow field – theory and experiment. In 'The Second International Symposium on Fire Safety Science', 13–17 June 1988, Tokyo, Japan. (Ed. T Wakamatsa) pp. 129–148. (International Association for Fire Safety Science: London, UK)

Cunningham P (2007) Idealised numerical simulations of the interactions between buoyant plumes and density currents. *Journal of the Atmospheric Sciences* **64**, 2105–2115. doi:10.1175/JAS3947.1

Drysdale D (1999) 'An Introduction to Fire Dynamics.' (Wiley: New York)

Ellis PF (2000) The aerodynamic and combustion characteristics of eucalypt bark – a firebrand study. PhD thesis, Australian National University, Canberra, ACT.

Ellis PFM (2010) The effect of the aerodynamic behaviour of flakes of jarrah and karri bark on their potential as firebrands. *Journal of the Royal Society of Western Australia* **93**, 21–27

Emmons H (1956) The film combustion of liquid fuel. *Zeitschrift für Angewandte Mathematik und Mechanik* **36**, 60–71. doi:10.1002/ZAMM.19560360105

Fernandez-Pello AC (1982) Analysis of the forced convective burning of a combustible particle. *Combustion Science and Technology* **28**, 305–313. doi:10.1080/00102208208952562

Fons WL (1946) Analysis of fire spread in light forest fuels. *Journal of Agricultural Research* **72**, 93–121.

Gould JS, McCaw WL, Cheney NP, Ellis PF, Knight IK, Sullivan AL (2009) 'Project Vesta – Fire Behaviour in Dry Eucalypt Forest: Fuel Structure, Fuel Dynamics and Fire Behaviour.' (Ensis–CSIRO: Canberra ACT; and Department of Environment and Conservation: Perth, WA)

Hanley DE, Cunningham P, Goodrick SL (2012) Interaction between a wildfire and the sea-breeze front. In 'Remote Sensing and Modeling Applications to Wildland Fire'. (Eds Qu JJ, Riebau AR, Yang RX, Sommers WT), pp. 78–95. (Springer–Verlag)

Himoto K, Tanaka T (2005) Transport of disk-shaped firebrands in a turbulent boundary layer. In 'The Eighth International Symposium on Fire Safety Science', 18–23 September 2005, Beijing, China. (Eds DT Gottuk, BY Lattimer) pp. 433–444. (International Association for Fire Safety Science: Baltimore, MD)

Hoerner SF (1958) 'Fluid-dynamic Drag; Practical Information on Aerodynamic Drag and Hydrodynamic Resistance.' (Hoerner Fluid Dynamics: Midland Park, NJ)

Kinoshita CM, Pagni PJ, Beier RA (1981) Opposed flow diffusion flame extensions. In 'The Eighteenth Symposium on Combustion', 16–22 August 1980, Waterloo, ON, Canada. pp. 1853–1860. (The Combustion Institute: Pittsburgh, PA)

Koo E (2008) 'Wildfire Modeling.' (VDM Verlag: Saarbrücken, Germany)

Koo E, Pagni PJ, Linn RR (2007) Using FIRETEC to describe firebrand behavior in wildfires. In 'The Tenth International Symposium of Fire and Materials', 29–31 January 2007, San Franscisco, CA. (Interscience Communications: London)

Koo E, Pagni PJ, Weise DR, Woycheese JP (2010) Firebrands and spotting ignitions in large-scale fires. *International Journal of Wildland Fire* **19**, 818–843. doi:10.1071/WF07119

Kortas S, Mindykowski P, Consalvi JL, Mhiri H, Porterie B (2009) Experimental validation of a numerical model for the transport of firebrands. *Fire Safety Journal* **44**, 1095–1102. doi:10.1016/J.FIRESAF.2009.08.001

Lee SL, Hellman JM (1969) Study of firebrand trajectories in a turbulent swirling natural convection plume. *Combustion and Flame* **13**, 645–655. doi:10.1016/0010-2180(69)90072-8

Lee SL, Hellman JM (1970) Firebrand trajectory study using an empirical velocity-dependent burning law. *Combustion and Flame* **15**, 265–274. doi:10.1016/0010-2180(70)90006-4

Linn RR (1997) A transport model for prediction of wildfire behavior. Los Alamos National Laboratory, Technical Report LA-13334-T. (Los Alamos, NM)

Linn RR, Cunningham P (2005) Numerical simulations of grass fires using a coupled atmosphere–fire model: basic fire behavior and dependence on wind speed. *Journal of Geophysical Research* **110**, D13107. doi:10.1029/2004JD005597

Linn RR, Reisner J, Colman JJ, Winterkamp J (2002) Studying wildfire behavior using FIRETEC. *International Journal of Wildland Fire* **11**, 233–246. doi:10.1071/WF02007

Linn RR, Winterkamp J, Colman JJ, Edminster C, Bailey JD (2005) Modeling interactions between fire and atmosphere in discrete-element fuel beds. *International Journal of Wildland Fire* **14**, 37–48. doi:10.1071/WF04043

Linn RR, Winterkamp J, Weise DR, Edminster C (2010) A numerical study of slope and fuel structure effects on coupled wildfire behaviour. *International Journal of Wildland Fire* **19**, 179–201. doi:10.1071/WF07120

Manzello SL, Cleary TG, Shields JR, Yang JC (2006*a*) Ignition of mulch and grasses by firebrands in wildland–urban interface fires. *International Journal of Wildland Fire* **15**, 427–431. doi:10.1071/WF06031

Manzello SL, Cleary TG, Shields JR, Yang JC (2006*b*) On the ignition of fuel beds by firebrands. *Fire and Materials* **30**, 77–87. doi:10.1002/FAM.901

Manzello SL, Maranghides A, Mell WE (2007) Firebrand generation from burning vegetation. *International Journal of Wildland Fire* **16**, 458–462. doi:10.1071/WF06079

Manzello SL, Cleary TG, Shields JR, Maranghides A, Mell W, Yang JC (2008*a*) Experimental investigation of firebrands: generation and ignition of fuel beds. *Fire Safety Journal* **43**, 226–233. doi:10.1016/J.FIRESAF.2006.06.010

Manzello SL, Shields JR, Cleary TG, Maranghides A, Mell WE, Yang JC, Hayashi Y, Nii D, Kurita T (2008b). On the development and characterization of a firebrand generator. *Fire Safety Journal* **43**, 258–268. doi:10.1016/J.FIRESAF.2007.10.001

Millán MM, Estrela MJ, Badenas C (1998) Meteorological processes relevant to forest fire dynamics on the Spanish Mediterranean coast. *Journal of Applied Meteorology* **37**, 83–100. doi:10.1175/1520-0450(1998)037<0083:MPRTFF>2.0.CO;2

Murazsew A (1974) Firebrand phenomena. The Aerospace Corporation, Report ATR-74(8165–01)-1. (El Segundo, CA)

Murazsew A, Fedele JB (1976) Statistical model for spot fire hazard. The Aerospace Corporation, Report ATR-77(7588)-1. (El Segundo, CA)

Murazsew A, Fedele JB (1977) Trajectory of firebrands in and out of fire whirls. *Combustion and Flame* **30**, 321–324. doi:10.1016/0010-2180(77)90081-5

Murazsew A, Fedele JB, Kuby WC (1975) Firebrand investigation. The Aerospace Corporation, Report ATR-75(7470)-1. (El Segundo, CA)

Nielsen HJ, Tao LN (1965) The fire plume above a large free-burning fire. In 'Tenth Symposium on Combustion', 17–21 August 1964, Cambridge, UK. pp. 965–972. (The Combustion Institute: Pittsburgh, PA)

Pagni PJ (1981) Diffusion flame analyses. *Fire Safety Journal* **3**, 273–285. doi:10.1016/0379-7112(81)90049-7

Pagni PJ (1993) Causes of the 20 October 1991 Oakland Hills conflagration. *Fire Safety Journal* **21**, 331–339. doi:10.1016/0379-7112(93)90020-Q

Pimont F, Dupuy JL, Linn RR, Dupont S (2009) Validation of FIRETEC wind-flows over a canopy and a fuel-break. *International Journal of Wildland Fire* **18**, 775–790. doi:10.1071/WF07130

Porterie B, Consalvi JL, Kaiss A, Loraud JC (2005) Predicting wildland fire behavior and emissions using a fine-scale physical model. *Numerical Heat Transfer Part A: Applications* **47**, 571–591. doi:10.1080/10407780590891362

Porterie B, Zekri N, Clerc J-P, Loraud J-C (2007) Modeling forest fire spread and spotting process with small world networks. *Combustion and Flame* **149**, 63–78. doi:10.1016/J.COMBUSTFLAME.2006.12.008

Reisner JM, Bossert J, Winterkamp J (1998) Numerical simulation of two wildfire events using a combined modeling system (HIGRAD/BEHAVE). In 'Second Symposium on Fire and Forest Meteorology of the American Meteorology Society', 11–16 January 1988, Phoenix, AZ. pp. 6–12. (American Meteorological Society: Boston, MA)

Reisner J, Wynne S, Margolin L, Linn R (2000) Coupled atmospheric–fire modeling employing the method of averages. *Monthly Weather Review* **128**, 3683–3691. doi:10.1175/1520-0493(2001)129<3683:CAFMET>2.0.CO;2

Sardoy N, Consalvi JL, Porterie B, Fernandez-Pello AC (2007) Modeling transport and combustion of firebrands from burning trees. *Combustion and Flame* **150**, 151–169. doi:10.1016/J.COMBUSTFLAME.2007.04.008

Sardoy N, Consalvi JL, Kaiss A, Fernandez-Pello AC, Porterie B (2008) Numerical study of ground-level distribution of firebrands generated by line fires. *Combustion and Flame* **154**, 478–488. doi:10.1016/J.COMBUSTFLAME.2008.05.006

Schaefer VJ (1957) The relationship of jet streams to forest wildfires. *Journal of Forestry* **55**, 419–425.

Sharples JJ (2009) An overview of mountain meteorological effects relevant to fire behaviour and bushfire risk. *International Journal of Wildland Fire* **18**, 737–754. doi:10.1071/WF08041

Spalding DB (1953) The combustion of liquid fuels. In 'Fourth Symposium on Combustion', 1–5 September 1952, Cambridge, MA. pp. 847–864. (The Combustion Institute: Pittsburgh, PA)

Tarifa CS, del Notario PP, Moreno FG (1965*a*) On flight paths and lifetimes of burning particles of wood. In 'Tenth Symposium on Combustion', 17–21 August 1964, Cambridge, UK. pp. 1021–1037. (The Combustion Institute: Pittsburgh, PA)

Tarifa CS, del Notario PP, Villa AR, Martinez L, Perez O (1965*b*) Open fires and transport of firebrands. Instituto Nacional de Tecnica Aeroespacial, Annual Technical Report, Grants FG-SP-114. (Madrid, Spain)

Tarifa CS, del Notario PP, Moreno FG, Villa AR (1967) Transport and combustion of firebrands. Instituto Nacional de Tecnica Aeroespacial, Final Technical Report, Grants FG-SP-114, FG-SP-146. (Madrid, Spain)

Tse SD, Fernandez-Pello AC (1998) On the flight paths of metal particles and embers generated by power lines in high winds – a potential source of wildland fires. *Fire Safety Journal* **30**, 333–356. doi:10.1016/S0379-7112(97)00050-7

Turns SR (2000) 'An Introduction to Combustion: Concepts and Applications.' (McGraw Hill: Boston, MA)

Wang H-H (2011) Analysis on downwind distribution of firebrands sourced from a wildland fire. *Fire Technology* **47**, 321–340. doi:10.1007/S10694-009-0134-4

White FM (1999) 'Fluid Mechanics.' (WCB/McGraw-Hill: Boston, MA)

Wilson R (1962) 'The Devil Wind and Wood Shingles: the Los Angeles Conflagration of 1961.' (National Fire Protection Association: Boston, MA)

Woycheese JP (1996) Brand lofting in large scale fires. MSc thesis, University of California Berkeley, CA.

Woycheese JP (2000) Brand lofting and propagation from large-scale fires. PhD thesis, University of California Berkeley, CA.

Woycheese JP (2001) Wooden disk combustion for spot fire spread. In 'The Ninth International Fire Science and Engineering Conference (INTER-FLAM)', 17–19 September, Edinburgh. pp. 101–112. (Interscience Communications: London)

Woycheese JP, Pagni PJ, Liepmann D (1998) Brand propagation from large-scale fires. In 'The Second International Conference of Fire Research and Engineering (ICFRE2)', 10–15 August 1997, Gaithersburg, MD. pp. 137–150. (Society of Fire Protection Engineers: Boston, MA)

Woycheese JP, Pagni PJ, Liepmann D (1999) Brand propagation from large-scale fires. *Journal of Fire Protection Engineering* **10**, 32–44. doi:10.1177/104239159901000203